Twitching motility suppressors reveal a role for FimX in type IV pilus extension dynamics

Nathan Roberge[1], Nathan Yuen[1], Hanjeong Harvey[1], Taylor J. Ellison[2], Courtney K. Ellison[2], and Lori L. Burrows[1]*

[1] Department of Biochemistry and Biomedical Sciences, and the Michael G. DeGroote Institute for Infectious Disease Research, McMaster University, Hamilton, ON, Canada, L8S4K1

[2] Department of Microbiology, University of Georgia, Athens, GA, 30602

*Corresponding author

lori.burrows@mcmaster.ca

Contributions

NR: Conceptualization, Investigation, Writing – original draft, Writing – review and editing

NY: Investigation, Writing – review and editing

HH: Resources, Writing – review and editing

TJE: Investigation, Writing – review and editing

CKE: Conceptualization, Investigation, Writing – review and editing

LLB: Conceptualization, Funding acquisition, Writing – original draft, Writing – review and editing

Abstract

In *Pseudomonas aeruginosa,* retractable protein filaments called type IV pili (T4P) facilitate surface adherence, sensing, and directional movement known as twitching motility. T4P are necessary for the bacteria to engage in surface-associated behaviors, including establishing acute infections. Pilus extension is driven by the hexameric ATPase, PilB, at the base of the T4P nanomachine in coordination with various protein regulatory effectors. The cyclic-di-GMP binding protein, FimX, works with PilB to mediate normal extension processes, though how this effector controls pilus assembly remains unclear. To explore the role of FimX in T4P function, we leveraged the significant Δ*fimX* twitching motility deficit to screen for mutants capable of overcoming this phenotype. We identified suppressor mutations that increase twitching in Δ*fimX* background, mapping primarily to cyclic-AMP homeostatic machinery or to PilB, the FimX target. Distinct suppressor mutations in PilB increased ATP hydrolysis *in vitro* and this activity was subject to modulation by FimX. Using microscopy to monitor the extension dynamics of fluorescently labelled T4P, we showed that Δ*fimX* mutants produce slow-to-extend, short pili, a phenotype that is rescued by mutations enhancing PilB ATP hydrolysis and/or re-introduction of FimX. Together, these data implicate FimX as a regulator of PilB enzymatic function, potentially enabling *P. aeruginosa* to fine-tune pilus extension dynamics in response to environmental cues.

Summary

Type IV pili enable *Pseudomonas aeruginosa* to attach to surfaces, move (twitch), and form biofilms. Pilus extension is powered by the motor protein PilB, which is regulated by other factors, including FimX, a protein that binds cyclic-di-GMP. Although FimX is important for twitching, how it influences PilB was unclear. We deleted *fimX*, which severely reduces motility,

53 and searched for mutants that regained movement. We identified two types: some had mutations
54 in PilB that increased its ATPase activity, allowing it to function without FimX, while others
55 affected the cyclic-AMP signaling pathway and increased overall production of pilus
56 components, showing that motility can also be improved through changes in quantity versus
57 quality. Our results suggest that FimX normally fine-tunes PilB enzymatic activity, enabling
58 dynamic control of pilus extension in response to surface signals. This work helps explain how
59 *P. aeruginosa* adapts to different environments, a process crucial for infection and biofilm
60 development.

61

62 **Introduction**

63 *Pseudomonas aeruginosa* deploys type IV pili (T4P) to adhere to and spread across
64 surfaces (1, 2). Directed bacterial movement, or twitching motility, is powered by repeated
65 cycles of protein filament extension, surface attachment, and retraction to pull cells along a
66 surface (3–5). Pilus function is coordinated through the action of four distinct protein
67 subcomplexes which together comprise the T4P nanomachine (Fig 1A) (6). T4P also allow cells
68 to sense surface contact and assist in the transition from planktonic to sessile lifestyles (5, 7–9),
69 facilitating microcolony formation, and eventually, biofilm production (10, 11). Engagement of
70 the extracellular filament with a surface induces an as-yet undefined signal that is propagated to
71 the inner membrane embedded Pil-Chp regulatory network, which in turn stimulates CyaB-
72 dependent synthesis of the secondary messenger molecule, cyclic adenosine monophosphate
73 (cAMP) (Fig 1A) (5, 7, 12). High intracellular cAMP activates the transcription factor Vfr to
74 modulate the expression of over 300 genes, including those encoding T4P machinery
75 components (13), with cAMP homeostasis maintained by the action of the CpdA
76 phosphodiesterase (14–16). The cascade of secondary messenger signaling culminates in

77 elevated cyclic diguanylate monophosphate (cdGMP) (16), which in many bacteria is associated
78 with sessile phenotypes such as biofilm formation (17). This increase in cdGMP potentially
79 occurs through stimulation of T4P-associated diguanylate cyclases (DGCs) like SadC (18, 19),
80 and/or through surface sensing by pilus tip-associated proteins (6, 16, 20, 21).

81 Pilus extension is an essential first step in filament biogenesis. Extended pili can interact
82 with external substrates, ultimately triggering downstream signaling and facilitating motility (2,
83 8, 22, 23). Extension is driven by the hexameric ATPase PilB (1, 24–26) in conjunction with
84 regulatory effectors PilZ (27, 28) and the cdGMP-binding protein FimX (27, 29–31) (Fig 1A),
85 both of which are necessary for normal pilus assembly. The role of FimX in pilus extension is
86 not well understood, with studies of *P. aeruginosa* FimX and its homologues in other species
87 implicating a variety of disparate functions (27, 30, 32, 33). In *P. aeruginosa*, FimX interaction
88 with PilB is contingent upon cdGMP binding by FimX's EVL motif in the C-terminal EAL
89 domain. *P. aeruginosa* FimX mutants that are unable to bind the secondary messenger are
90 defective in surface piliation (30, 31), twitching motility (29–31), and ATPase localization (27,
91 30). Some of these phenotypes can be overcome through suppressor mutations that increase
92 cellular cdGMP levels. Those studies suggest that FimX is responsible for maintaining PilB
93 functional efficiency over broad concentrations of cdGMP (31). On the other hand, more recent
94 work showed selective trafficking of the PilB-FimX subcomplex to the leading poles of
95 twitching cells. This localization promotes biased pilus extension at a single pole, resulting in
96 increased Pil-Chp network signaling at the same pole. The positive feedback loop was proposed
97 to ensure directional movement of the rod-shaped cells in response to PilB localization. Further,
98 PilB polar localization was dependent upon FimX and various cytoplasmic components of the

99 Pil-Chp network, suggesting that FimX may also be a cdGMP-binding polar localization factor
100 that coordinates optimal PilB subcellular distribution (8, 34).

101 How then, do these proposed functions intersect and what is the role of FimX in *P.*
102 *aeruginosa* pilus function and/or signaling? To shed light on how FimX controls pilus function,
103 we leveraged the Δ*fimX* twitching motility deficit to select for suppressor mutants capable of
104 overcoming loss of its input. Our screen revealed two classes of mutants with increased motility
105 in the absence of FimX. These mutations were primarily in the Pil-Chp network responsible for
106 modulating cAMP levels or PilB, the interaction partner of FimX. We focused on the PilB
107 mutations, which notably were not clustered but rather mapped to various regions of the protein.
108 We characterized two distinct examples and demonstrated that each significantly increased PilB
109 ATP hydrolysis *in vitro*. Phenotypically, this elevated activity translated to increased rates of
110 extension, resulting in longer pili. Both ATPase activity and pilus extension rates were subject to
111 FimX-dependent modulation. Therefore, FimX modulates PilB enzymatic efficiency to produce
112 longer pili suited for twitching motility.

113

114 **Results**

115 **Suppressor mutations restore motility in Δ*fimX* mutants**

116 FimX is a regulator of pilus extension in *P. aeruginosa*, though its exact mechanism is
117 not well understood (29–31). Consistent with previous work, we confirmed that a PAO1 deletion
118 mutant of *fimX* had significantly reduced twitching motility, 5-10% of the wild type (Fig 1B).
119 However, this strain still twitched when compared to a non-motile major pilin (*pilA*::Tn5) mutant
120 and remained susceptible to the pilus-targeting bacteriophage, PO4 (Fig 1C). FimX mutants did
121 not produce detectable surface pili in sheared protein fractions (Fig S1), further supporting a

122 defect in pilus extension. This phenotype is distinct from that of mutants lacking another PilB
123 regulator, the putative chaperone, PilZ (27, 28), which do not twitch and are resistant to pilus-
124 specific phages (Fig 1B and C).

125 We reasoned that we could leverage the Δ*fimX* pilus extension deficit to screen for
126 suppressor mutants capable of restoring twitching motility, to inform on the function of FimX.
127 After allowing *fimX* mutants to twitch at the sub-agar interface for an extended period (48-72 h),
128 we isolated highly motile flares that emerged from the small primary twitching zone (Fig 1D).
129 These cells were collected, isolated for single colonies, and after confirming their increased
130 motility compared to the Δ*fimX* parent, were sequenced to identify candidate suppressor
131 mutations. The mutations mapped to relevant proteins including the ATPase PilB, alignment
132 subcomplex component PilO (35, 36), members of the Pil-Chp network (PilJ and FimL) (7), and
133 CpdA (additional mutants are listed in Table S1). Each mutation increased motility to varying
134 degrees (Fig 1E), though not to wild-type levels, but did not impact growth (Fig S2) or phage
135 susceptibility (Fig S3). Complementing the suppressor mutants with *fimX* further increased
136 twitching motility to levels similar to or greater than WT, except for PilO P168L, suggesting it
137 has a *fimX* independent motility phenotype (Fig S4A). In contrast, complementation of the
138 suppressors with a defective version of FimX – where its cdGMP-binding EVL motif was
139 mutated to AAA – did not further increase twitching motility, consistent with previous reports
140 that this non-functional variant is incapable of PilB binding (30). Diminished twitching motility
141 in the WT strain when FimX AAA was expressed in trans is likely due to formation of FimX-
142 FimX AAA heterodimers, supported by their pairwise interactions in a bacterial 2-hybrid assay
143 (Fig S4B).

144

145 **Δ*fimX* suppressor mutations do not directly influence cdGMP metabolism**

146 Previous efforts to isolate Δ*fimX* suppressors revealed several mutations which
147 collectively upregulated intracellular cdGMP levels (31). To test whether our mutants shared this
148 phenotype, we assessed intracellular levels of cdGMP using a *pcdrA*:Lux cassette-based reporter
149 system in liquid cultures (20). Under these conditions, none of our mutants demonstrated higher
150 cdGMP levels over time when compared to control cells expressing the well-characterized
151 diguanylate cyclase (DGC), SadC (Fig 2A). To directly test the impact of cdGMP on Δ*fimX*
152 suppression, we overexpressed DGCs from *P. aeruginosa* (*sadC*) or *Escherichia coli* (*ydeH*) in
153 WT or Δ*fimX* backgrounds and tested twitching motility. In all cases, cells expressing the DGCs
154 showed significantly reduced twitching motility compared to the vector control (Fig 2B).
155 Together, these data suggest that suppression of the Δ*fimX* motility defect in PAO1 is not related
156 to changes in cdGMP levels.

157

158 **Elevated cAMP levels increase motility in the Δ*fimX* background**

159 Since several of our motile suppressor mutations mapped to the Pil-Chp network or
160 CpdA, we hypothesized that changes to cAMP homeostasis (5, 7) increased twitching in the
161 absence of *fimX*. We therefore assessed intracellular levels of cAMP in both liquid cultures and
162 surface-adapted cellular populations using a *PaQa*:YFP reporter plasmid system (37). WT cells
163 had significantly higher levels of cAMP when the cells were grown on a surface versus in liquid,
164 but elevated cAMP-dependent signal was lost in a *pilA* mutant (Fig 3A), consistent with T4P
165 being a major input to cAMP generation in *P. aeruginosa* (38). Deletion of CyaB or expression
166 of a constitutively active CyaB R456L *in trans* further reduced or increased cAMP levels,

167 respectively (15, 39, 40). In these assay conditions, Δ*fimX* had lower than WT levels of cAMP
168 and was unable to respond to surface contact. The Δ*fimX* suppressor mutants PilJ T570I, FimL
169 L115F, and CpdA V258G all had significantly elevated cAMP levels. In contrast, neither the
170 PilB nor PilO P168L suppressor mutants had significant increases in cAMP levels compared to
171 the Δ*fimX* parent. These data suggested that there were at least two routes to increase twitching
172 in the *fimX* background, one of which was independent of cAMP levels.

173 We next asked whether high cAMP levels were responsible for increased Δ*fimX*
174 twitching. Expressing CyaB from a multicopy plasmid in the Δ*fimX* background was sufficient to
175 significantly increase twitching motility compared to the empty vector control (Fig 3B), while
176 expression of an inactive CyaB variant (Fig S5A) (41) was not. This increased twitching
177 phenotype was also observed in a double mutant lacking the Pil-Chp response regulators PilG
178 and PilH (Fig S5B), bypassing Pil-Chp-dependent CyaB activation (34). Together, these data
179 indicate that elevated cAMP levels due to Pil-Chp or CpdA mutations increase Δ*fimX* motility.
180 Strains with high intracellular cAMP in turn had increased Vfr-dependent expression (13) of an
181 mRuby3 fluorescent protein reporter integrated upstream of the T4P *pilMNOPQ* operon (Fig
182 3C). Integration of the reporter did not impact phage susceptibility of these strains (Fig S6)
183 indicating that pilus function is maintained. Consistent with this increased expression, levels of
184 PilO were also elevated (Fig 3D) suggesting that more T4P machines are expressed in these
185 backgrounds.

186 Notably, the PilB and PilO suppressors had no increase in Vfr-dependent transcription or
187 abundance of T4P components (Fig 2C and D) compared to Δ*fimX*, consistent with low cAMP
188 levels (Fig 3A). Another cAMP-dependent trait, type II secretion system-dependent secretion of
189 proteases generating zones of clearing on skim-milk plates (42) was also unchanged (Fig S7A

190 and B), collectively suggesting that the cAMP levels in those mutants were not significantly
191 impacted (13, 15), and that Δ*fimX* suppression occurs through non-cAMP related mechanisms in
192 these backgrounds.

193

194 **Determinants for *pilB* Δ1bp function**

195 The suppressors in the non-cAMP related class predominantly mapped to the pilus
196 extension ATPase, PilB. To probe this second set, we focused first on a mutant in which a single
197 adenine was deleted in the last codon of the PilB open reading frame (*pilB* Δ1bp). This deletion
198 produced a frameshift that extended the coding sequence by an additional 21 bases, or seven
199 amino acids, to the next stop codon (Fig 4A). When modelled in Alphfold3, the extended
200 segments were predicted to be solvent-exposed, protruding from the base of the hexamer and
201 away from its putative interaction interfaces with additional T4P components (Fig S8). To find
202 the minimum length of this C-terminal extension that was sufficient to increase motility in
203 Δ*fimX*, we generated single codon truncations from the 3′ end of the *pilB* Δ1bp sequence (Fig
204 4A). Each variant complemented motility in both a *pilB*::Tn5 background (Fig S9A), and in the
205 WT (Fig S9B), confirming that they produced a functional gene product with no dominant
206 negative effect through mixed oligomerization with WT PilB. In a strain lacking both *pilB* and
207 *fimX*, all *pilB* Δ1bp truncations tested significantly increased twitching motility relative to the
208 control complemented with WT PilB (Fig 3B). Notably, longer extensions rescued motility to a
209 greater degree than shorter ones.

210 Interestingly, the shortest *pilB* Δ1bp-21 truncation was identical in length to WT PilB, yet
211 only the *pilB* Δ1bp-21 sequence significantly increased twitching motility in the double mutant

212 (Fig 4B). Only the C-terminal amino acid differs between the two, with a valine substituted for
213 an aspartate in the *pilB* Δ1bp-21 sequence. PilB D566 may therefore play an important role in
214 modulating the function of the enzyme. The longer *pilB* Δ1bp sequences that support increased
215 motility have additional positively charged residues (Fig 4A), suggesting that loss of negative
216 charge at the C-terminus enhances PilB function. Since the above studies were done with
217 multicopy plasmids, we next introduced single chromosomal point mutants at the PilB C-
218 terminus in a Δ*fimX* background to assess recovery of twitching motility. A PilB D566V
219 mutation significantly increased twitching motility compared to the Δ*fimX* parent (Fig 4C). We
220 also observed a significant increase in twitching when the C-terminal amino acid was charge-
221 swapped to a lysine, but not when we introduced glutamate (Fig 4C). The second-last amino acid
222 in the native PilB sequence is a positively charged lysine, and we hypothesized that shortening
223 the WT sequence by a single amino acid to expose the positive charge would also restore
224 motility in a Δ*fimX* mutant. However, substituting D566 with a stop codon did not significantly
225 increase motility relative to the control (Fig 4C). These data suggest that PilB C-terminal charge,
226 in addition to C-terminal length, is an important regulator of PilB function.

227

228 **Determinants for PilB T430P function**

229 We next examined a second PilB suppressor (PilB T430P) which mapped to a site distal
230 to the C-terminus (Fig S8). A multiple protein sequence alignment of full-length PilB
231 homologues from various species revealed that the region surrounding T430 was well conserved,
232 although T430 itself was not (Fig 4D). We therefore reasoned that this amino acid was less
233 important to overall PilB function or potentially a species-specific regulatory site. We made
234 individual substitutions at T430, choosing amino acids found at this position in the other

235 homologues. All mutant constructs complemented twitching motility in a *pilB*::Tn5 background
236 and the WT (Fig S10). In a *pilB fimX* double mutant, only the original T430P suppressor
237 supported twitching motility (Fig 4E). Therefore, disruption of local PilB secondary structure,
238 rather than specific side-chain chemistry, is likely responsible for increased motility.

239 An Alphafold3 model of a PilB monomer predicted that residue T430 is located in the
240 second turn of a short α-helix (Fig 4D and S8). While T430 is not well conserved, other amino
241 acids in this helical segment, such as an adjacent R431, are. Alignment of the model onto the
242 crystal structure of hexameric PilB from *Geobacter metallireducens* bound to a non-hydrolysable
243 ATP analogue shows that the equivalent N429 (T430) and R430 (R431) residues are positioned
244 at the protomer-protomer interface or jutting into the lumen of the torus, depending on the phase
245 of the ATP hydrolysis cycle (Fig S8). We hypothesized that this secondary structural element
246 could be involved in inter-subunit communication and that the introduction of a helix-breaking
247 proline would alter these functional contacts. Supporting this idea, mutation of the adjacent
248 residues to proline, L429P or R431P, significantly increased twitching motility in *fimX pilB* (Fig
249 4F). In contrast, R431A failed to increase motility in the double mutant, thus disruption of the α-
250 helical segment rather than loss of this sidechain chemistry was likely responsible for altering
251 PilB function. Interestingly, in the *pilB*::Tn5 or WT backgrounds where FimX was present (Fig
252 S11A and B), twitching motility of PilB R431A and R431P variants was significantly decreased
253 compared to control (Fig S11A). Therefore, the presence or absence of FimX modulates the
254 function of these PilB variants.

255

256

257 **Increased twitching of suppressors is due to enhanced PilB ATPase activity**

258 We next investigated how the *pilB* Δ1bp and PilB T430P mutations restored pilus
259 function in a Δ*fimX* background. Other PilB regulatory effectors, such as PilZ, are thought to
260 serve as molecular chaperones and *pilZ* mutants lack detectable intracellular PilB on Western
261 blots (Fig 5A). This is consistent with results from previous studies of the *Xanthomonas citri*
262 PilZ homologue (27). The *pilZ* mutants are also non-motile and phage resistant (Fig 1B and C),
263 in keeping with their negligible levels of PilB. In contrast, PilB was still detectable in Δ*fimX* or
264 FimX AAA backgrounds, although its levels were approximately half of WT (Fig 5A). Neither
265 suppressor increased levels of PilB compared to those in Δ*fimX* or FimX AAA. Since FimX is
266 important for PilB polar localization (8, 27, 30), the reduction in PilB levels in *fimX* mutants may
267 be a consequence of fewer interactions between the ATPase and T4P machinery, making it more
268 susceptible to degradation.

269 Since PilB is an ATPase used to power pilus extension, we reasoned that the mutations
270 might increase enzymatic activity. PilB has two N-terminal domains (N1D and N2D) connected
271 by a flexible linker to the C-terminal domain (Figure S8) (43). The N1D can be removed without
272 disrupting hexamer formation to improve stability and solubility for *in vitro* studies (27, 44–48).
273 We purified ΔN1D-PilB variants to assess ATP hydrolysis efficiency *in vitro* (Fig S12). Both
274 PilB suppressors hydrolyzed significantly more ATP than the WT and catalytically inactive
275 Walker A mutant (PilB K332A) (1) controls over time (Fig 5B), as well as following overnight
276 incubation (Fig 5C). Despite mapping to disparate sites in the protein, both PilB suppressors
277 upregulated enzymatic activity and likely compensate for loss of FimX through this shared
278 mechanism. Interestingly, when we added FimX and cdGMP to the reaction, we saw a decrease
279 in ATP hydrolysis for *pilB* Δ1bp but an increase for PilB T430P (Fig 5D). While this result is

280 difficult to interpret, it suggests that FimX can modulate PilB enzymatic activity. In a genetic
281 context, *pilB* Δ1bp and PilB T430P mutations integrated into the chromosome restored twitching
282 motility to at least WT levels in the presence of FimX (Fig 5E), but not FimX AAA. Taken
283 together, this indicates that these PilB suppressor mutants can continue to respond to cdGMP-
284 bound FimX input and regulation.

285

286 **FimX promotes pilus extension to produce longer pili**

287 To test the impact of increased ATP hydrolysis by PilB on pilus assembly, we imaged
288 pilus dynamics using fluorescence microscopy (Fig 6A). The major pilin subunit, PilA, was first
289 labelled with a fluorescent maleimide dye at A86C as previously described (4, 49). All PilA
290 A86C mutants remained motile with slightly reduced twitching compared to the wild type (Fig
291 S13). WT cells produced T4P at the cell poles as expected, with some cells producing pili at both
292 poles (Fig 6A). Notably, the Δ*fimX* mutant produced very short pili that were difficult to detect,
293 often presenting only as bright polar puncta which we scored as a polar accumulation of labelled
294 PilA or very short T4P, below the limit of detection. In addition, fewer cells were piliated
295 compared to WT (Fig 6B and C). We chose to quantify pili using the Δ*fimX pilB* Δ1bp mutant as
296 this strain showed the most robust twitching phenotype of our suppressors. Furthermore, in the
297 presence of FimX, the *pilB* Δ1bp mutation alone had greater than WT levels of twitching,
298 providing an optimal background to study FimX's functional contribution. In the Δ*fimX pilB*
299 Δ1bp background, piliation was restored on many cells (Fig 6B and C), with longer pili
300 compared to the Δ*fimX* mutant (Fig 6A). The percentage of piliated cells in the Δ*fimX pilB* Δ1bp
301 mutant was similar to WT (Fig 6B and C), but the average maximum pilus length was
302 significantly shorter (Fig 6D), likely explaining its comparatively reduced motility (Fig 5E).

303 Maximum pilus length was significantly increased compared to the Δ*fimX* parent, indicating that
304 the *pilB* Δ1bp mutation caused cells to produce longer pili, presumably through enhanced ATP
305 hydrolysis. The *pilB* Δ1bp alone background produced the longest pili (Fig 6A and D) and had
306 the highest percentage of piliated cells (Fig 6B and C), consistent with this strain being the most
307 motile (Fig 5E). Longer and long-lived pili in PAO1 (~2-3 μm) comprise a rare subpopulation
308 (4). We therefore anticipate that more Δ*fimX* cells are likely piliated, but since the maximum
309 pilus length in these mutants is ~0.75 μm, most pili may not be detectable.

310 The *pilB* Δ1bp mutants afforded an opportunity to quantify pilus dynamics in the
311 presence or absence of FimX. We quantified the rates of pilus extension and retraction over time
312 in the Δ*fimX pilB* Δ1bp versus *pilB* Δ1bp to assess FimX's contribution to pilus dynamics. The
313 FimX-expressing strain had a significantly increased average rate of pilus extension (Fig 6E)
314 while the average rate of retraction was not significantly different, supporting FimX's role as a
315 modulator of PilB-dependent pilus extension. These data suggest that FimX directly increases
316 pilus extension efficiency, likely by acting on PilB.

317 In *P. aeruginosa* and other bacterial species, fluorescently labelled FimX fusions display
318 defects in polar localization when PilB interaction is impaired (27, 30, 33). Consistent with these
319 other studies, most Δ*fimX* mutant cells complemented with an N-terminal fusion of mNeonGreen
320 (mNGr) to FimX showed bright puncta localized to a single cell pole (Fig 7A), with a smaller
321 population of cells displaying bipolarly-distributed puncta (Fig 7B). The WT FimX fusion also
322 complemented twitching motility (Fig S14A), while cells expressing an empty vector control had
323 no discernable puncta (Fig S14B). The number of cells with identifiable polar puncta was
324 decreased by ~20-50% when *pilB* was deleted or if a mNGr-FimX AAA fusion was used (Fig

325 7B). Importantly, these data indicate that FimX localization patterns in our strains are consistent
326 with previous reports (8, 27, 30) and are contingent on interaction with PilB.

327

328 **PilB enhancing mutations are uncommon**

329 Given the relative ease of selection for *fimX* suppressor mutations that mapped to PilB
330 and improved twitching motility, we wondered if similar PilB mutations were common in
331 sequenced strains of *P. aeruginosa*. We compared 417 PilB orthologue sequences from the
332 Pseudomonas.com database to identify comparable mutations. Of these, 297 were the same
333 length as PAO1 PilB at 566 residues, and 82 were longer. Of those sequences, 72 were longer by
334 one residue, 8 by two residues, 1 by four residues, and 1 by 15 residues (Fig S15A). Strikingly,
335 despite these differences in length, the C-terminal residue of all sequences was an aspartic acid.
336 We also assessed the local sequence surrounding PilB T430 for helix-disrupting residues which
337 may confer a similar effect to T430P. We examined the region +/- three amino acids from the
338 residue aligned with PAO1 PilB T430 in a full-length protein sequence alignment, to capture the
339 most likely positions to influence stability of a 3-turn α-helix. Of the 417 sequences, 4 had a
340 proline residue and 8 had a glycine within this window, accounting for less than 1% and 2% of
341 the total sequences respectively (Fig S15B). This analysis of *P. aeruginosa* sequences suggests
342 that PilB mutations similar to the ones identified in this screen are uncommon.

343

344 **Discussion**

345 The reason that optimal PilB function in *P. aeruginosa* needs the regulatory input of
346 FimX remains poorly understood (30, 31). To address this knowledge gap, we screened for
347 suppressors capable of overcoming the Δ*fimX* motility deficit. We identified several suppressor

348 mutants, most of which mapped to the Pil-Chp network or to PilB (Table S1). A previous Tn-Seq
349 screen used to isolate suppressors in *P. aeruginosa* strain PA103 implicated FimX as a sensor of
350 the secondary messenger cdGMP. In that strain, Δ*fimX* suppressors with high levels of cdGMP
351 had increased motility, leading the authors to posit that FimX senses internal cdGMP to tune
352 pilus assembly efficiency over broad concentrations of the molecule (31). Unexpectedly, we
353 found no suppressors in cdGMP homeostatic machinery, nor did any of our mutations increase
354 cdGMP synthesis (Fig 2A). Further, exogenous expression of DGCs also failed to alleviate the
355 Δ*fimX* motility defect in PAO1 (Fig 2B), unlike in PA103 Δ*fimX* where expression of the
356 unrelated DGC PleD from *Caulobacter crescentus* was sufficient to restore motility and surface
357 piliation. While these phenotypic discrepancies may be strain-specific, overexpression of other
358 DGCs in PAO1 was reported to suppress twitching motility, though surface piliation was not
359 significantly impacted (31). Why these strains behave differently in response to cdGMP
360 production is not yet clear.

361 Instead, we found that increases in the secondary messenger cAMP increased twitching
362 in Δ*fimX*, though this is likely an indirect mechanism. Increasing the levels of cAMP drives
363 transcription of the Vfr regulon, which includes T4P components. Mutations that promote
364 accumulation of cAMP lead to the expression of additional pilus machines. Given that Δ*fimX*
365 mutants retain the ability to twitch, albeit poorly, these high cAMP mutants likely produce an
366 abundance of sub-optimally functioning T4P machines which cumulatively improve the cells'
367 ability to twitch (Fig 8). A similar pattern of compensation via elevated cAMP production was
368 recently reported for suppressors of another modulator of pilus function in strain PA14 (50).

369 We also isolated a suppressor that mapped to PilO (PilO P168L), a member of the T4P
370 alignment subcomplex (35). Notably, this mutant was the only one tested that was not

371 complemented to at least WT twitching by FimX expression (Fig S4). Therefore, the twitching
372 recovery mechanism for this mutant is likely independent of the FimX-PilB extension pathway.
373 PilO interacts with regulatory components such as SadC (18) and may connect pilus function to
374 environmental signals.

375 The suppressor mutations in PilB provided a useful tool to study FimX-dependent
376 physiology. Despite mapping to separate sites (Fig S8), both mutations increased ATP hydrolysis
377 (Fig 5A and B) suggesting that one of FimX's roles may be to enhance PilB enzymatic activity.
378 For the *pilB* Δ1bp mutant, mechanistic clues come from structural work on other extension
379 ATPases. The C-terminal solvent-exposed face of the *G. metallireducens* PilB hexamer has
380 dispersed negative surface charge (25, 26). The extended Δ1bp C-termini, which include several
381 positively charged residues, are predicted to protrude into this environment (Fig S8). Increasing
382 positive charge, or removing the native C-terminal negative charge, could promote electrostatic
383 stabilization of the hexamer, or facilitate the PilB conformational changes necessary for substrate
384 hydrolysis.

385 Analysis of the PilB T430P mutant uncovered a novel regulatory region in the PilB
386 multimer. Disruption of the short helix containing T430 restored twitching motility in a Δ*fimX*
387 background. The adjacent R431 residue is highly conserved in PilB homologues, and an R431P
388 variant increased twitching in Δ*fimX* but interestingly, significantly attenuated motility in the
389 presence of FimX (Fig S11). These PilB mutants therefore continue to interact with and respond
390 to FimX, though resulting in different functional outcomes. This secondary structural element
391 may represent an intramolecular regulatory site involved in FimX recognition or perhaps is
392 involved in communicating conformational changes induced through FimX interaction. More
393 detailed biochemical studies are still required to unravel these possibilities.

394 In the absence of FimX, twitching is diminished. Using fluorescence microscopy, we
395 showed that the pili of *fimX* mutants are significantly shorter than WT (Fig 6D). This result is
396 consistent with low levels of surface pili in sheared protein fractions (Fig S1). The Δ*fimX pilB*
397 Δ1bp suppressor mutant had increased PilB ATP hydrolysis and produced longer pili,
398 presumably through increased PilA polymerization. These data suggest that twitching motility in
399 PAO1 is maximized when cells make longer pili, as WT and *pilB* Δ1bp strains generated the
400 longest pili and largest twitching zones. When comparing Δ*fimX pilB* Δ1bp and *pilB* Δ1bp, we
401 saw a significant increase in the rate of pilus extension, but not retraction (Fig 6E). Our data
402 therefore support a model where FimX-PilB interaction stimulates pilus extension, potentially by
403 stabilizing or promoting the PilB conformational changes necessary to drive pilus assembly
404 within the stator (Fig 8). In *X. citri*, the addition of FimX stimulated ATP hydrolysis by a PilB-
405 PilZ complex *in vitro* (27). We also showed that FimX influenced *P. aeruginosa* ΔN1D-PilB
406 function *in vitro* (Fig 5D), implying that the two proteins interact. In other bacteria, FimX is
407 thought to engage the extension machinery through PilZ (27, 33, 51, 52). Similar FimX-PilZ
408 interactions have not been detected in *P. aeruginosa* (53), however, leaving definition of the
409 specific interaction interfaces for future studies.

410 In *P. aeruginosa* and *Xanthomonas spp*., FimX has also been proposed to function as a
411 PilB polar localization factor (8, 27, 30), rather than as a chaperone like PilZ. In *P. aeruginosa*,
412 FimX shows polar localization defects in *pilB* backgrounds or when it is unable to bind to
413 cdGMP (Fig 7), suggesting that both cdGMP-bound FimX and PilB are required for polar co-
414 localization (30). The mechanism behind polar trafficking is poorly understood, but recent
415 evidence suggested that the Pil-Chp response regulator PilG was essential for proper PilB polar
416 localization (8, 34). Consistent with these observations, a recent study in *Acinetobacter baylyi*

417 demonstrated that its FimX homologue controls T4P localization through interactions with
418 components of the Pil-Chp pathway, but that this localization is independent of cdGMP binding
419 (32). How those factors are targeted to the cell poles in *P. aeruginosa* remains an open question.
420 PilB and FimX may first need to form a complex which is then recognized by additional factors
421 such as PilG. Alternatively, FimX interaction may bias PilB polar occupancy or keep it
422 sequestered, ensuring that the leading pole is primed for multiple rounds of pilus assembly (Fig
423 8). In this scenario, PilB and FimX polar retention is mutually contingent, but FimX instead
424 functions to reduce disengagement of PilB from active T4P machinery.

425 In other bacteria such as *Vibrio* or *Neisseria* species, pili are used predominantly for
426 surface adhesion (54, 55), cell-cell contact (56), DNA uptake (57, 58), or biofilm formation (55).
427 These organisms lack obvious FimX homologues. Instead, the N-terminal domain of extension
428 ATPases in these species binds directly to cdGMP, and nucleotide binding is essential for
429 function (54, 59–61). Pilus extension is therefore optimal at high intracellular cdGMP
430 concentrations, but this condition suppresses twitching motility. In *P. aeruginosa,* nucleotide
431 binding to FimX, which then dictates PilB localization and function, may serve as a functional
432 alternative. As a high affinity sensor of cdGMP (29, 33), FimX may drive optimal pilus
433 extension rates to enable multiple dynamic cycles of pilus assembly, and therefore facilitate
434 twitching, in response to nucleotide availability. This organization might also explain why
435 mutations which enhance PilB function are rare in *P. aeruginosa*, as these may dysregulate pilus
436 functional responses to signaling cues.

437

438

439

440 **Materials and Methods**

441

442 **Bacterial strains and growth conditions**

443 All strains and plasmids used in this study are outlined in Table S2. Bacterial strains were
444 grown aerobically at 37 °C in Lysogeny Broth (LB) media (10 g/L tryptone, 5 g/L yeast extract,
445 and 5 g/L NaCl), supplemented with the appropriate concentration of antibiotics where necessary
446 unless otherwise specified. Antibiotics were used at the following concentrations: 15 µg/mL or
447 30 µg/mL of gentamicin for *E. coli* or *P. aeruginosa* respectively unless otherwise indicated. 50
448 µg/mL or 200 µg/mL kanamycin for *E. coli* or *P. aeruginosa* respectively. 100 µg/mL of
449 ampicillin or 200 µg/mL of carbenicillin for *E. coli* or *P. aeruginosa* respectively. Plasmid
450 constructs were generated using *E. coli* DH5α before introduction into the appropriate cellular
451 background by heat shock (*E. coli*) or electroporation (*P. aeruginosa* or *E. coli*) where
452 appropriate.

453

454 **Plasmid and strain construction**

455 Fragments of interest were PCR amplified from isolated mPAO1 genomic DNA. All
456 PCR primers are listed in Table S3. For point mutations, two separate PCR amplified DNA
457 fragments were stitched together through a second single overlap extension PCR, with each
458 DNA overhang including the mutation of interest introduced during primer synthesis. For
459 plasmid construction, the in-frame genetic insert and corresponding vector were digested with
460 the appropriate FastDigest restriction enzymes (ThermoFisher Scientific) as per manufacturer
461 instruction and ligated with T4 DNA ligase. Ligated products were transformed via heat shock
462 into *E. coli* DH5α and selected on 1.5% agar LB media plates supplemented with the appropriate

463 antibiotic. Following selection, single colonies were harvested, and the plasmid was mini
464 prepped using a GeneJet plasmid prep kit (ThermoFisher Scientific) for sequence confirmation
465 (Plasmidsaurus).

466 Genetic manipulation of mPAO1 chromosomal DNA was performed by double
467 homologous recombination as previously described (62). In brief, for genetic deletions, ~500 bp
468 upstream and downstream of the desired target sequence were PCR amplified and purified from
469 isolated PAO1 genomic DNA. Upstream and downstream sequences were engineered to contain
470 ~50-100 bases of the 5′ or 3′ ends of the gene deletion target to ensure minimal disruption of
471 adjacent genes. Upstream and downstream fragments were digested with the appropriate
472 restriction enzymes along with the suicide vector backbone pEX18Gm. Digested fragments were
473 ligated using T4 ligase and transformed into via heat shock into *E. coli* DH5α and selected for on
474 1.5% agar LB media plates supplemented with gentamicin. Purified and sequenced plasmids
475 were then transformed into *E. coli* SM10 (λ*pir*). A single colony of SM10 harbouring the
476 plasmid was grown overnight in 3 mL of LB media supplemented with gentamicin. The
477 following day, the SM10 culture was mixed with the appropriate strain of mPAO1 overnight
478 culture in a 1:1 ratio (by volume), pelleted by centrifugation, the resulting cell pellet was
479 resuspended in 50 µL of LB and then spotted on 1.5% agar LB plates dried in a biological safety
480 cabinet for 20-30 min. The spot was allowed to dry at room temperature before being incubated
481 at 37 °C overnight. The following day, the cell spot was scraped into fresh LB media and plated
482 onto premixed *Pseudomonas* isolation agar (Difco) supplemented with 100 µg/mL of
483 gentamicin. The plates were incubated again at 37 °C overnight. Single colonies were then re-
484 streaked again on *Pseudomonas* isolation agar plates supplemented with 100 µg/mL of
485 gentamicin and incubated overnight at 37 °C. The next day, cells were streaked in a zig-zag

486 pattern on 10% LB (1 g/L tryptone, 0.5 g/L yeast extract) with no added NaCl, 1.5% agar, and
487 5% sucrose media plates and incubated overnight at 37 °C. Single colonies from the sucrose
488 media selection plate were patched again onto a fresh sucrose media plate as well as an LB
489 media plate supplemented with gentamicin. Patches which grew on sucrose media but not LB
490 with gentamicin were assessed for chromosomal deletion via colony PCR.

491 For chromosomal knock-in of a point mutation, the same protocol as outlined above was
492 performed only differing at initial construct design. Knock-in constructs were instead generated
493 ~500 bp upstream or downstream of the mutation site through single overlap extension PCR.
494 Overlap extension primers were also designed to silently introduce or remove a restriction cut
495 site in the genome where applicable to facilitate downstream quality assurance. The remaining
496 procedure was then carried out as described.

497

498 **Twitching motility assays**

499 Bacterial strains were streaked onto 1.5% agar LB media plates supplemented with
500 gentamicin where applicable and grown overnight at 37 °C. The following day, cells were picked
501 using a sterile pipette tip and stabbed down to the bottom layer plastic of 1% agar LB media
502 tissue culture treated plates, supplemented with antibiotic or arabinose where applicable, dried
503 for 30 min in a biological safety cabinet. Plates were incubated overnight at 37 °C. The
504 following day, the agar was carefully removed with a pipette tip and discarded. The twitching
505 zones adhered to the plate were stained with 0.1% crystal violet dye for a minimum of 10 min,
506 washed twice with DI water, and left to air dry overnight at room temperature before imaging

507 with a scanner. Twitching zone areas were then digitally traced using ImageJ, and either
508 duplicates or triplicates were averaged.

509

510 **Phage-susceptibility assays**

511 Bacterial strains were inoculated into 3 mL of LB media liquid cultures and grown
512 overnight at 37 °C. The next morning, 5 µL of overnight culture was sub-cultured into 3 mL of
513 fresh LB media and grown at 37 ºC to mid-logarithmic phase (OD_{600} ~0.5-1.0). Cells were
514 normalized to an OD_{600} of 0.1 in LB. For plate-based assays, 10 µL of bacterial suspension was
515 mixed with 5 µL of serially diluted PO4 phage stock (3e5 PFU/mL original titer). 10 µL of cell-
516 serial phage dilution was spotted onto 1.5% agar LB media dried for 30 min in a biological
517 safety cabinet. The plate was incubated overnight at room temperature. The following day, the
518 plate was incubated again at 37 °C for 2-3 hours before imaging with a scanner.

519 For liquid-based assays, 2 µL of OD_{600} normalized cell suspension was added to 200 µL
520 of LB media total in a flat bottom 96 well plate. To each well, 1 µL of 3e5 PFU/mL PO4 phage
521 stock was also added. The plate lid was sealed with masking tape and then incubated overnight
522 in a 37 °C shaking plate reader, with OD_{600} readings taken every 30 min for 16-18 hours. Curves
523 were normalized to LB media blank wells in the same plate.

524

525 **Sheared surface protein preparation**

526 Surface pilin and flagellin protein levels were assessed as previously described (63).
527 Briefly, strains were streaked in grid-like pattern on a 1.5% agar LB media plate dried for 30

528 minutes in a biological safety cabinet. The plate was incubated at 37 ºC overnight. The next
529 morning, cells were gently scrapped off the surface using a combination of a glass coverslip and
530 sterile inoculation loop into 1.2 mL of sterile 1X PBS. Surface appendages were sheared by
531 vortexing the suspension for 30 s. The homogenized suspension was transferred to a 1.5 mL
532 Eppendorf tube and pelleted by centrifugation at maximum speed for 30 min. The supernatant
533 was decanted into a fresh tube and 0.1 volume of 5M NaCl and 30% (w/v) polyethylene glycol
534 (MW range 8k) was added. The tubes were then incubated on ice for 90 min, inverting the tubes
535 periodically. The precipitated protein was collected by centrifugation again for 30 min at
536 maximum speed. The supernatant was decanted, and the precipitated protein resuspended in 50
537 µL of 1X SDS loading dye (62.5 mM Tris-HCl pH 6.8, 0.5% (w/v) SDS, 5% (v/v) β-
538 mercaptoethanol, 10% (v/v) glycerol, 0.25% (w/v) bromophenol blue), and boiled for 10 min.
539 The tubes were centrifuged for another 5 min at maximum speed and separated on a 15% SDS-
540 polyacrylamide gel. Proteins were visualized with Coomassie blue staining.

541

542 **Bacterial 2-hybrid assay**

543 Single colonies of *E. coli* BTH101 co-transformed with both T18/T25 tagged target
544 proteins were inoculated into 3 mL LB media overnight cultures supplemented with kanamycin,
545 ampicillin, and 0.5 mM IPTG. The following morning, the cultures were normalized to an OD_{600}
546 of 0.1 in fresh LB and 4 µL was spotted onto MacConkey agar plates (40 g/L, Difco)
547 supplemented with kanamycin, ampicillin, 0.5 mM IPTG, and 1% maltose pre-dried for 40 min
548 in a biological safety cabinet. The spots were allowed to dry at room temperature before
549 incubation at 30 ºC in a standing incubator. The plates were imaged after 24 hours.

550 **Selecting Δ*fimX* twitching suppressor mutants**

551 Motility suppressors were isolated through the standard twitching assay described with
552 some alterations. Δ*fimX* bacteria were first streaked for single colonies on an LB agar plate.
553 Using a sterile pipette tip, a single colony was stab-inoculated into a standard twitching plate ~4-
554 5 times in a row. The tip was discarded, and a new colony was then stab inoculated in the same
555 manner. This was repeated for a total of 35-40 individual twitching zones on a single assay plate.
556 The plate was sealed with parafilm and incubated at 37 ºC for 48-72 hours. Following
557 incubation, the top agar layer was carefully removed and discarded. Flares emerging from small
558 twitching zones were collected with a sterile cotton swab and streaked again for single colonies.
559 Single mutant colonies were reassessed for twitching motility. Those with increased twitching
560 relative to the Δ*fimX* strain were collected and their genomic DNA isolated using a Wizard
561 genomic DNA isolation kit (Promega) as per manufacturer's instructions. Isolated chromosomal
562 DNA was sent for Illumina Sequencing (SeqCenter) and mutations were identified using BreSeq
563 (64). Where appropriate, candidate mutations were reintroduced into the chromosome as
564 described above.

565

566 **cdGMP reporter assay**

567 The cdGMP reporter assay was conducted as previously described (20) with some
568 alterations. Briefly, cells transformed with the reporter construct (*pcdrA*:LuX-PMS402) were
569 grown in LB media liquid cultures supplemented with kanamycin (as well as gentamicin for the
570 high control carrying *sadC*-pBADGr) overnight at 37 ºC. Overnight cultures were diluted (1:25)
571 in 3 mL of fresh LB media with antibiotics and grown at 37 ºC to mid-logarithmic phase.

572 Cultures were then normalized to an OD_{600} of 0.1 and 2 µL of suspension was added to 200 µL
573 of LB media total supplemented with antibiotics in a black flat clear-bottom 96 well plate. The
574 plate was sealed with masking tape and then incubated overnight in a 37 °C shaking plate reader,
575 with chemiluminescence and OD_{600} readings taken every 15 min for 16-18 hours. Relative
576 luminescence signal was normalized to OD_{600} reading at the same timepoint.

577

578 **cAMP reporter assay**

579 The cAMP reporter assay was conducted as previously described (37) with some
580 alterations. Briefly, cells transformed with the reporter construct (*rpoD*:mKate/*PaQa*:YFP –
581 O'Toole Lab) were grown in LB media liquid cultures supplemented with carbenicillin (as well
582 as gentamicin for the high cAMP control carrying CyaB R456L-pBADGr) overnight at 37 ºC.
583 Overnights were sub-cultured 1:25 in 5 mL of M8 minimal media containing 0.2% glucose,
584 0.5% casamino acids, and 1 mM $MgSO_4$ supplemented with carbenicillin to an OD_{600} of 0.2-0.4.
585 At this point, 200 µL of liquid culture was spread onto 1% agar M8 media plates dried for 20
586 min in a biological safety cabinet. Liquid cultures and plates were then incubated for an
587 additional 5 hours at 37 ºC. After the incubation, 1 mL of sterile PBS was added to each plate
588 and cells were scraped up with a sterile inoculation loop. 100 µL of cell suspension was taken
589 from each plate and normalized to an OD_{600} of ~0.2 in sterile 1X PBS. The liquid cultures were
590 also normalized to an OD_{600} of ~0.2 in sterile 1X PBS. 200 µL of normalized cell suspensions
591 were then added to a black flat clear bottom 96 well plate (Corning). mKate (Ex: 588/Em: 635)
592 and YFP (Ex: 500/Em: 541) fluorescence were measured, and the signal was normalized by
593 dividing YFP/mKate for both surface-adapted and liquid samples.

594 **Vfr reporter assay**

595 For *vfr* promoter activity detection, cells harbouring a gene encoding mRuby3
596 chromosomally integrated upstream of *pilM* and under control of the *pilMNOPQ* promoter were
597 streaked onto 1.5% agar LB media plates and incubated overnight at 37 ºC. The next morning,
598 cells were harvested into sterile 1X PBS and normalized to an OD_{600} of ~0.1. 200 µL of cell
599 suspension was then added to a black flat clear bottom 96 well plate. mRuby3 (Ex: 558/Em: 600)
600 fluorescence and exact OD_{600} were then measured, and the signal was normalized by dividing
601 mRuby3/OD_{600}.

602

603 **Western blot analysis**

604 Whole cell lysates were first separated on a 15% or 12% SDS-polyacrylamide gels for
605 PilA and PilB respectively. Samples were transferred to a nitrocellulose membrane at 225 mA
606 for 1 hour. The membranes were blocked with 5% (w/v) skim milk (Bioshop) dissolved in 1X
607 Tris-buffered saline (TBS: 20 mM Tris-HCl pH 7.6, 150 mM NaCl) overnight or for 2 hours for
608 PilA or PilB respectively. Primary incubation was performed as previously described using
609 rabbit antisera (65). The membranes were washed 4 times for 5 min with 1X TBS before
610 incubation using alkaline phosphatase-conjugated goat-anti rabbit IgG secondary antibody
611 (BioRad) in a 1:3500 dilution. The membranes were washed 4 times with 1X TBS and developed
612 using alkaline phosphatase developing reagent according to manufacturer's protocol, before
613 imaging the membranes in an Azure Biosystems 400 transilluminator.

614

615

616 **Skim milk T2SS secretion assay**

617 Liquid cultures were grown overnight in LB media at 37 ºC. The next morning, each
618 culture was normalized to an OD_{600} of 0.2 and spotted onto tryptic soy agar plates supplemented
619 with 1.5% skim milk powder (Bioshop) dried for 30 min in a biological safety cabinet. The spots
620 were allowed to dry at room temperature before incubation overnight at 37 ºC. The resulting
621 zones of clearance were then imaged with a scanner and the zone areas were quantified digitally
622 using ImageJ.

623

624 **Protein modelling and sequence alignments**

625 Alphafold3 was used to predict protein structures and generate predicted aligned error
626 plots using the unmodified default settings (66). All models and plots were visualized in UCSF
627 ChimeraX (67). Full length PilB sequences were aligned using Geneious Prime and visualized
628 using ESPript3 (68).

629

630 **Protein purification**

631 N-terminally truncated PilB (ΔN1D-PilB: M1-D180) and full length FimX were
632 subcloned into pET28b with an N-terminal His_6-tag for inducible expression. PilB was purified
633 as previously described with some alterations. Briefly, ΔN1D-PilB expressing overnight cultures
634 of BL21-CodonPlus (DE3)-RIL were sub-cultured (1:100) in 1 L of LB supplemented with
635 kanamycin and incubated at 37 ºC with shaking until mid-logarithmic phase (~0.4-0.8 OD_{600}).
636 Cells were induced with 0.5 mM IPTG overnight at 18ºC with shaking. The next morning, cells

637 were harvested by centrifugation at 3000 xg for 20 min. Cell pellets were resuspended in lysis
638 buffer (50 mM HEPES pH 7.3, 250 mM NaCl, 10 mM imidazole) and incubated on ice with
639 20mg of lysozyme for 15 min with periodic inversion. Cells were then lysed using sonication and
640 the supernatant clarified through centrifugation at 31000 xg for 30 min. Supernatant was then
641 incubated with ~5 mL of Ni^{2+}-NTA resin (Millipore) pre-equilibrated with lysis-buffer for 1 hour
642 on ice with gentle shaking. The resin was washed with 3 separate 30 mM imidazole washes (15
643 mL) before elution with 250 mM imidazole. The elution fraction was dialyzed overnight at 4 ºC
644 into 7.3 mM HEPES pH 7.3, 200 mM NaCl and concentrated using an Amicon concentrator
645 (Millipore-Sigma). Protein was then aliquoted, flash frozen in liquid nitrogen, and stored at -
646 80ºC. FimX was expressed as described above and purified as previously described (30), except
647 for the final purification step involving separation by size-exclusion chromatography (Superdex
648 200, Cytiva) equilibrated using 50 mM Tris-HCl pH 8.0, 250 mM NaCl, and 5 mM β-ME.
649 Protein-containing fractions were determined using SDS-PAGE and then pooled for
650 concentration using an Amicon concentrator.

651

652 **ATPase activity assay**

653 All ATPase assays contained equimolar amount of ΔN1D-PilB or mutants (100 nM) to
654 ensure valid comparison. PilB reaction buffer was prepared containing 50 mM HEPES pH 7.3,
655 200 mM NaCl, 5 mM $MgCl_2$, 1 μM $ZnCl_2$, and 1 mM ATP. Where applicable, the reaction
656 buffer was supplemented with 1 μM cdGMP, and/or 200 nM of purified FimX. Aliquots of
657 ΔN1D-PilB was thawed and the tube was centrifuged at maximum speed for 10 min at 4 ºC to
658 pellet insoluble precipitate. The remaining supernatant was transferred to a fresh tube and kept
659 on ice. ATPase reactions were performed in a clear flat-bottom 96 well plate (Corning) in a total

660 volume of 100 µL at 37 ºC in a standing incubator. Following incubation and at the appropriate
661 time point, 50 µL of reaction was mixed with 100 µL of BioMol green reagent (Enzo
662 Lifesciences) incubated at room temperature for 15 min at which point absorbance at 620 nm
663 was read with a spectrophotometer. Each ΔN1D-PilB reaction series was normalized to the
664 timepoint at 0 min to ensure consistent background signal reduction. For overnight incubations,
665 the 96-well plate lid was sealed with masking tape, and the reaction was performed as described
666 with samples being normalized to an equivalent reaction well lacking PilB.

667

668 **Fluorescence microscopy experiments**

669 T4P labeling experiments were performed using a cysteine knock-in method described
670 previously, with some species-specific changes (4, 69). 100 µl of overnight cultures of *P.*
671 *aeruginosa* were spotted onto prewarmed LB agar plates and grown upright at 37 °C for 4-5
672 hours. Plate-grown cells were then scraped off of plates using a P200 pipette tip and gently
673 resuspended into 100 µl of fresh LB. AlexaFluor488-maleimide (Sigma) was added to the cell
674 suspension for a final concentration of 50 ng/µl and incubated for 45-60 min in the dark at room
675 temperature. Cells were washed once with 200 µl fresh LB using centrifugation settings of
676 18,000 x *g* for 1 min. Cell were resuspended into 200 µl of fresh LB. mNeonGreen-FimX strains
677 were prepared exactly the same way except with gentamycin supplemented in the medium and
678 with no AlexaFluor488-maleimide labeling steps. All imaging was performed under 1% agarose
679 pads made with PBS solution. Cell bodies were imaged using phase-contrast microscopy on a
680 Nikon Ti2-E microscope using a Plan Apo 100X oil immersion objective, a GFP/FITC/Cy2 filter
681 set for pili and mNeonGreen-FimX, a Hamamatsu ORCA-Fusion Gen-III cCMOS camera, and
682 Nikon NIS Elements Imaging Software. Measurements of pili were quantified manually using

683 Fiji. Notably, populations of *P. aeruginosa* containing labeled T4P exhibit variability in labeling
684 efficiency for unknown reasons. Therefore, T4P fluorescence signal contrast was adjusted so that
685 T4P were clearly visible for each strain.

686

687 **Acknowledgements**

688 We thank Dr. George O'Toole and Dr. Christopher Geiger for the cAMP reporter
689 plasmid and their help in optimizing the detection assay. We thank Dr. Lynne Howell and Ian
690 Yen for the *ydeH*-pBADGr plasmid. We also thank Dr. Sara Andres, Caitlin Doubleday, and the
691 Andres lab for access to equipment and assistance in purifying all proteins used in this study. We
692 thank the members of the Burrows lab for their helpful discussions and insights. This work was
693 supported by a Canadian Institutes of Health Research Project grant (PJT-156080) to LLB and a
694 National Institutes of Health grant (R35GM150916) to CKE. LLB holds a Tier 1 Canada
695 Research Chair in Microbe-Surface Interactions (CRC 2021–00103). CKE is a Damon Runyon-
696 Marilyn and Scott Urdang Breakthrough Scientist supported by the Damon Runyon Cancer
697 Research Foundation (DFS6023). NR holds an NSERC CGS-D award. NY was funded through
698 an NSERC USRA.

699
700
701
702
703
704
705
706
707

Figure Captions

Figure 1: Suppressor mutations overcome Δ*fimX* twitching motility defects. (A) The type IV pilus nanomachine comprising four distinct protein subcomplexes (motor, alignment, secretin subcomplexes, and pilus fiber) and associated inner-membrane Pil-Chp signaling network responsible for cAMP generation. PilB in association with regulatory effectors PilZ and FimX drives pilus extension. **(B)** Quantification of sub-agar stab twitching motility zones for extension regulatory effector mutants. Representative crystal violet-stained twitching zones are shown to the left. X-axis depicts a $\log_2$ scale. Bars represent the means of triplicate samples from three independent experiments ± SD. **(C)** Representative plaque assay demonstrating 10-fold serial dilutions of bacteriophage PO4 on extension regulatory effector mutants. **(D)** Cartoon representation of the Δ*fimX* suppressor mutant screen setup. A representative motile flare is shown to the right. Image border = 1 cm. **(E)** Quantification of sub-agar stab twitching motility zones for selected Δ*fimX* suppressor mutants. Representative twitching zones are shown to the left. Data are plotted as a fold change of the Δ*fimX* parent strain. Bars represent the means of triplicate samples from three independent experiments ± SD. All scale bars = 1 cm. ***: $p \leq 0.001$ (Two-tailed parametric *t*-test).

Figure 2: FimX suppressor mutations do not impact intracellular cdGMP levels. (A) Time-course curves of relative luminesence signal of a *pcdrA*:LuX cassette cdGMP reporter normalized to OD_{600}. Each timepoint is the mean of triplicate samples from three independent experiments ± SD. **EV**: empty pMS402 vector, ***sadC***: *sadC* in pBADGr vector. **(B)** Quantification of sub-agar stab twitching motility zones for strains overexpressing diguanylate cyclases (DGCs). Representative crystal violet-stained twitching zones are shown to the left. DGC expression was induced with 0.1% arabinose. Bars represent the means of triplicate samples from three independent experiments ± SD. X-axis depicts a $\log_2$ scale. Scale bar = 1 cm. **EV**: empty pBADGr vector, ***sadC***: *sadC* in pBADGr vector, ***ydeH***: *ydeH* in pBADGr vector. ***: $0.001 \geq p$ (Two-tailed parametric *t*-test).

Figure 3: A subset of Δ*fimX* twitching suppressors elevate cAMP levels and upregulate associated phenotypes. (A) Plasmid-based cAMP reporter assay quantifying cAMP-dependent YFP expression (*PaQa*) normalized to constitutive mKate expression (*rpoD*). Bars represent the means of duplicate samples from three independent experiments ± SD. **(B)** Quantification of sub-agar stab twitching motility zones for strains overexpressing the adenylate cyclase CyaB or a catalytically inactive mutant. Representative crystal violet-stained twitching zones are shown to the left. Expression was induced with 0.1% arabinose. Bars represent the means of triplicate samples from three independent experiments ± SD. Scale bar = 1 cm. **EV**: empty pHERD30T vector, **His_6-CyaB (D234S)**: N-terminally hexa-histidine tagged CyaB or CyaB D234S in pHERD30T vector. **(C)** Vfr-dependent expression of mRuby3 chromosomally inserted upstream of the native alignment complex *pilMNOPQ* operon. Bars represent the means of duplicate samples from three independent experiments ± SD. Cartoon schematic of the mRuby3 expression system is shown above the graph. **(D)** Representative PilO Western blot. Sample

750 loading was normalized to a non-specific band shown below. Molecular weight is indicated to
751 the left. Blot is representative of three independent experiments. **CyaB R456L**: CyaB R456L in
752 pBADGr vector. *: $0.05 \geq p \geq 0.01$; **: $0.01 \geq p \geq 0.001$; ***: $0.001 \geq p$ (Two-tailed parametric
753 *t*-test).

754

755 **Figure 4: PilB mutations increase twitching motility in the absence of *fimX*. (A)** Cartoon
756 schematic of deleted base pair A1697 at the PilB C-terminus, shown in red, and resulting
757 extended sequence. The *pilB* Δ1bp truncation sequences are shown below. **(B)** Quantification of
758 twitching zone areas of Δ*fimX pilB*::Tn5 double mutants overexpressing *pilB* Δ1bp 3′
759 truncations. Representative crystal violet stained twitching zones are shown to the left. PilB
760 expression was induced with 0.05% arabinose. Bars represent the means of duplicate samples
761 from three independent experiments ± SD. **(C)** Quantification of twitching zone areas of Δ*fimX*
762 PilB D566X point mutants chromosomal knock-ins. Representative twitching zones are shown to
763 the left. Bars represent the means of triplicate samples from three independent experiments ± SD.
764 **(D)** Full-length multiple sequence alignment of PilB homologues from various species
765 highlighting the sequence surrounding PAO1 PilB T430, labelled in red. The Alphafold3 model
766 of the predicted secondary structure in this region is shown to the left. **(E)** Quantification of
767 twitching zone areas of *fimX pilB* double mutants overexpressing PilB T430X mutants.
768 Representative twitching zones are shown to the left. PilB expression was induced with 0.05%
769 arabinose. Bars represent the means of duplicate samples from three independent experiments ±
770 SD. **(F)** Quantification of twitching zone areas of *fimX pilB*::Tn5 double mutants overexpressing
771 PilB constructs with point mutations in positions adjacent to T430. Representative twitching
772 zones are shown to the left. PilB expression was induced with 0.05% arabinose. Bars represent
773 the means of triplicate samples from three independent experiments ± SD. **EV**: empty
774 pHERD30T vector, ***pilB* Δ1bp-3 to 21**: *pilB* Δ1bp-3 to 21 in pHERD30T vector, **PilB**
775 **L429/T430/R431X**: indicated PilB substitution in pHERD30T vector. All scale bars = 1 cm. **ns**:
776 $p \geq 0.05$; *: $0.05 \geq p \geq 0.01$; **: $0.01 \geq p \geq 0.001$; ***: $0.001 \geq p$ (Two-tailed parametric *t*-test).

777

778 **Figure 5: PilB suppressor mutations increase ATP hydrolysis. (A)** Representative PilB
779 Western blot. Sample loading was normalized to a non-specific band shown below. Molecular
780 weight is indicated to the left. Blot is representative of three independent experiments.
781 Quantification using BioMol green reagent of free phosphate released over a time course **(B)** or
782 following overnight incubation **(C)** by ΔN1D-His_6-PilB-catalyzed ATP hydrolysis. PilB K332A,
783 a non-catalytically active Walker mutant, was used as a negative control. **(D)** Quantification of
784 free phosphate release by ΔN1D- His_6-PilB-catalyzed ATP hydrolysis in the presence of cdGMP
785 containing reaction buffer (+Buffer) or with cdGMP and FimX (+FimX) following overnight
786 incubation. **(E)** Quantification of twitching zone areas of Δ*fimX* or FimX AAA mutants with or
787 without individual PilB suppressor mutation chromosomal knock-ins. Representative crystal
788 violet stained twitching zones are shown to the left. Bars represent the means of triplicate
789 samples from three independent experiments ± SD. Scale bar = 1 cm. **ns**: $p \geq 0.05$; *: $0.05 \geq p \geq$
790 0.01; **: $0.01 \geq p \geq 0.001$; ***: $0.001 \geq p$ (Two-tailed parametric *t*-test).

Figure 6: FimX mutants produce short pili due to slow extension rates. (A) Representative images of PilA A86C type IV pili labelled with maleimide-Alexafluor 488 with background fluorescence subtracted. White arrows indicate visible pili. All scale bars = 2 µm. Number of cells producing visible PilA A86C type IV pili expressed as a percentage of total cells **(B)** or normalized relative to the WT arbitrarily set to 1 **(C)**. Bars represent the means ± SD of three independent experiments (WT n = 193, Δ*fimX* n = 181, Δ*fimX pilB* Δ1bp n = 210, *pilB* Δ1bp n = 197 total cells). Technical replicates are indicated by colour. **(D)** Maximum PilA A86C pilus length. Each sample depicts the means ± SD of three independent experiments, each point represents a single PilA A86C pilus length (WT, Δ*fimX pilB* Δ1bp, and *pilB* Δ1bp n = 60, Δ*fimX* n = 45 total pili). Technical replicates are indicated by colour. **(E)** Rate of PilA A86C pilus extension or retraction. Each sample depicts the means ± SD of three independent experiments, each point represents the rate of extension and/or retraction of a single PilA A86C pilus (Δ*fimX pilB* Δ1bp n = 46, *pilB* Δ1bp n = 44 total extension and Δ*fimX pilB* Δ1bp n = 40, *pilB* Δ1bp n = 41 total retraction events). **ns**: $p \geq 0.05$; *****: $0.05 \geq p \geq 0.01$; ******: $0.01 \geq p \geq 0.001$ (Two-tailed parametric *t*-test).

Figure 7: FimX polar localization is disrupted in the absence of PilB binding. (A) Representative images of cells expressing an mNeonGreen N-terminal FimX or FimX AAA fusion with background fluorescence subtracted. All scale bars = 2 µm. **(B)** Quantification of cells expressing an mNeonGreen-N-terminal FimX or FimX AAA fusion scored for bipolar, unipolar, or no discernable puncta and expressed as a percentage of total cells. Bars represent the means ± SD of three independent experiments (Δ*fimX* + mNGr-FimX n= 216, Δ*fimX pilB*::Tn5 + mNGr-FimX n= 213, Δ*fimX* + mNGr-FimX AAA n= 235, Δ*fimX pilB*::Tn5 + mNGr-FimX AAA n= 206, total cells). **mNGr-FimX** or **mNGr-FimX AAA**: mNeonGreen N-terminal FimX or FimX AAA fusion in pHERD30T vector. Expression was not induced with arabinose.

Figure 8: Model of Δ*fimX* suppression pathways. Suppression of the Δ*fimX* twitching motility deficit can occur through mutations which elevate intracellular levels of the secondary messenger molecule cAMP. More cAMP generation leads to increased Vfr-dependent expression of T4P components, which assemble into more machines, increasing twitching motility. This mechanism is not FimX-specific. Alternatively, mutations that increase PilB ATP hydrolysis lead to production of longer pili. This overcomes the short-pilus defect observed in *fimX* mutants. FimX in complex with PilB enhances the rate of PilB-dependent pilus extension to produce longer pili optimized for twitching motility. FimX polar localization to T4P machines is contingent on PilB binding, therefore FimX influences its polar trafficking and/or sequestration.

References

1. Chiang, P., Sampaleanu, L. M., Ayers, M., Pahuta, M., Howell, P. L., and Burrows, L. L. Y. 2008 Functional role of conserved residues in the characteristic secretion NTPase motifs of the *Pseudomonas aeruginosa* type IV pilus motor proteins PilB, PilT and PilU. *Microbiology*. **154**, 114–126
2. Burrows, L. L. (2012) *Pseudomonas aeruginosa* twitching motility: type IV pili in action. *Annu. Rev. Microbiol.* **66**, 493–520
3. Jakovljevic, V., Leonardy, S., Hoppert, M., and Søgaard-Andersen, L. (2008) PilB and PilT Are ATPases Acting Antagonistically in Type IV Pilus Function in *Myxococcus xanthus*. *J. Bacteriol.* **190**, 2411–2421
4. Koch, M. D., Fei, C., Wingreen, N. S., Shaevitz, J. W., and Gitai, Z. (2021) Competitive binding of independent extension and retraction motors explains the quantitative dynamics of type IV pili. *Proc. Natl. Acad. Sci. U. S. A.* **118**, e2014926118
5. Persat, A., Inclan, Y. F., Engel, J. N., Stone, H. A., and Gitai, Z. (2015) Type IV pili mechanochemically regulate virulence factors in *Pseudomonas aeruginosa*. *Proc. Natl. Acad. Sci.* **112**, 7563–7568
6. Guo, S., Chang, Y., Brun, Y. V., Howell, P. L., Burrows, L. L., and Liu, J. (2024) PilY1 regulates the dynamic architecture of the type IV pilus machine in *Pseudomonas aeruginosa*. *Nat. Commun.* **15**, 9382
7. Inclan, Y. F., Persat, A., Greninger, A., Von Dollen, J., Johnson, J., Krogan, N., Gitai, Z., and Engel, J. N. (2016) A scaffold protein connects type IV pili with the Chp chemosensory system to mediate activation of virulence signaling in *Pseudomonas aeruginosa*. *Mol. Microbiol.* **101**, 590–605
8. Kühn, M. J., Talà, L., Inclan, Y. F., Patino, R., Pierrat, X., Vos, I., Al-Mayyah, Z., Macmillan, H., Negrete, J., Engel, J. N., and Persat, A. (2021) Mechanotaxis directs *Pseudomonas aeruginosa* twitching motility. *Proc. Natl. Acad. Sci. U. S. A.* **118**, e2101759118
9. Laventie, B.-J., Sangermani, M., Estermann, F., Manfredi, P., Planes, R., Hug, I., Jaeger, T., Meunier, E., Broz, P., and Jenal, U. (2019) A Surface-Induced Asymmetric Program Promotes Tissue Colonization by *Pseudomonas aeruginosa*. *Cell Host Microbe*. **25**, 140-152.e6
10. Comolli, J. C., Hauser, A. R., Waite, L., Whitchurch, C. B., Mattick, J. S., and Engel, J. N. (1999) *Pseudomonas aeruginosa* Gene Products PilT and PilU Are Required for Cytotoxicity In Vitro and Virulence in a Mouse Model of Acute Pneumonia. *Infect. Immun.* **67**, 3625–3630
11. O'Toole, G. A., and Kolter, R. (1998) Flagellar and twitching motility are necessary for *Pseudomonas aeruginosa* biofilm development. *Mol. Microbiol.* **30**, 295–304
12. Fulcher, N. B., Holliday, P. M., Klem, E., Cann, M. J., and Wolfgang, M. C. (2010) The *Pseudomonas aeruginosa* Chp Chemosensory System Regulates Intracellular cAMP Levels by Modulating Adenylate Cyclase Activity. *Mol. Microbiol.* **76**, 889–904
13. Wolfgang, M. C., Lee, V. T., Gilmore, M. E., and Lory, S. (2003) Coordinate regulation of bacterial virulence genes by a novel adenylate cyclase-dependent signaling pathway. *Dev. Cell*. **4**, 253–263

14. Kim, H.-S., Kim, S.-M., Lee, H.-J., Park, S.-J., and Lee, K.-H. (2009) Expression of the cpdA gene, encoding a 3',5'-cyclic AMP (cAMP) phosphodiesterase, is positively regulated by the cAMP-cAMP receptor protein complex. *J. Bacteriol.* **191**, 922–930
15. Fuchs, E. L., Brutinel, E. D., Klem, E. R., Fehr, A. R., Yahr, T. L., and Wolfgang, M. C. (2010) In Vitro and In Vivo Characterization of the *Pseudomonas aeruginosa* Cyclic AMP (cAMP) Phosphodiesterase CpdA, Required for cAMP Homeostasis and Virulence Factor Regulation. *J. Bacteriol.* **192**, 2779–2790
16. Luo, Y., Zhao, K., Baker, A. E., Kuchma, S. L., Coggan, K. A., Wolfgang, M. C., Wong, G. C. L., and O'Toole, G. A. (2015) A Hierarchical Cascade of Second Messengers Regulates *Pseudomonas aeruginosa* Surface Behaviors. *mBio*. **6**, e02456-14
17. Jenal, U., Reinders, A., and Lori, C. (2017) Cyclic di-GMP: second messenger extraordinaire. *Nat. Rev. Microbiol.* **15**, 271–284
18. Webster, S. S., Lee, C. K., Schmidt, W. C., Wong, G. C. L., and O'Toole, G. A. (2021) Interaction between the type 4 pili machinery and a diguanylate cyclase fine-tune c-di-GMP levels during early biofilm formation. *Proc. Natl. Acad. Sci.* **118**, e2105566118
19. Merritt, J. H., Ha, D.-G., Cowles, K. N., Lu, W., Morales, D. K., Rabinowitz, J., Gitai, Z., and O'Toole, G. A. (2010) Specific Control of *Pseudomonas aeruginosa* Surface-Associated Behaviors by Two c-di-GMP Diguanylate Cyclases. *mBio*. **1**, 10.1128/mbio.00183-10
20. Marko, V. A., Kilmury, S. L. N., MacNeil, L. T., and Burrows, L. L. (2018) *Pseudomonas aeruginosa* type IV minor pilins and PilY1 regulate virulence by modulating FimS-AlgR activity. *PLOS Pathog.* **14**, e1007074
21. Webster, S. S., Mathelié-Guinlet, M., Verissimo, A. F., Schultz, D., Viljoen, A., Lee, C. K., Schmidt, W. C., Wong, G. C. L., Dufrêne, Y. F., and O'Toole, G. A. (2022) Force-Induced Changes of PilY1 Drive Surface Sensing by *Pseudomonas aeruginosa*. *mBio*. **13**, e03754-21
22. Harvey, H., Bondy-Denomy, J., Marquis, H., Sztanko, K. M., Davidson, A. R., and Burrows, L. L. (2018) *Pseudomonas aeruginosa* defends against phages through type IV pilus glycosylation. *Nat. Microbiol.* **3**, 47–52
23. Koch, M. D., Black, M. E., Han, E., Shaevitz, J. W., and Gitai, Z. (2022) *Pseudomonas aeruginosa* distinguishes surfaces by stiffness using retraction of type IV pili. *Proc. Natl. Acad. Sci.* **119**, e2119434119
24. Collins, R., Karuppiah, V., Siebert, C. A., Dajani, R., Thistlethwaite, A., and Derrick, J. P. (2018) Structural cycle of the *Thermus thermophilus* PilF ATPase: the powering of type IVa pilus assembly. *Sci. Rep.* **8**, 14022
25. McCallum, M., Tammam, S., Khan, A., Burrows, L. L., and Howell, P. L. (2017) The molecular mechanism of the type IVa pilus motors. *Nat. Commun.* **8**, 15091
26. McCallum, M., Burrows, L. L., and Howell, P. L. (2019) The Dynamic Structures of the Type IV Pilus. *Microbiol. Spectr.* 10.1128/microbiolspec.PSIB-0006-2018
27. Llontop, E. E., Cenens, W., Favaro, D. C., Sgro, G. G., Salinas, R. K., Guzzo, C. R., and Farah, C. S. (2021) The PilB-PilZ-FimX regulatory complex of the Type IV pilus from *Xanthomonas citri*. *PLOS Pathog.* **17**, e1009808
28. Alm, R. A., Bodero, A. J., Free, P. D., and Mattick, J. S. (1996) Identification of a novel gene, *pilZ*, essential for type 4 fimbrial biogenesis in *Pseudomonas aeruginosa*. *J. Bacteriol.* **178**, 46–53

919 29. Kazmierczak, B. I., Lebron, M. B., and Murray, T. S. (2006) Analysis of FimX, a
920 phosphodiesterase that governs twitching motility in *Pseudomonas aeruginosa*. *Mol.*
921 *Microbiol.* **60**, 1026–1043
922 30. Jain, R., Sliusarenko, O., and Kazmierczak, B. I. (2017) Interaction of the cyclic-di-GMP
923 binding protein FimX and the Type 4 pilus assembly ATPase promotes pilus assembly.
924 *PLOS Pathog.* **13**, e1006594
925 31. Jain, R., Behrens, A.-J., Kaever, V., and Kazmierczak, B. I. (2012) Type IV Pilus Assembly
926 in *Pseudomonas aeruginosa* over a Broad Range of Cyclic di-GMP Concentrations. *J.*
927 *Bacteriol.* **194**, 4285–4294
928 32. Ellison, T. J., Yen, I. Y., Howell, P. L., and Ellison, C. K. (2025) FimX regulates type IV
929 pilus localization via the Pil-Chp chemosensory system in *Acinetobacter baylyi*.
930 10.1101/2025.05.21.655318
931 33. Wei, C., Wang, S., Liu, P., Cheng, S.-T., Qian, G., Wang, S., Fu, Y., Qian, W., and Sun, W.
932 (2021) The PdeK-PdeR two-component system promotes unipolar localization of FimX and
933 pilus extension in *Xanthomonas oryzae* pv. *oryzicola*. *Sci. Signal.* **14**, eabi9589
934 34. Kühn, M. J., Macmillan, H., Talà, L., Inclan, Y., Patino, R., Pierrat, X., Al-Mayyah, Z.,
935 Engel, J. N., and Persat, A. (2023) Two antagonistic response regulators control
936 *Pseudomonas aeruginosa* polarization during mechanotaxis. *EMBO J.* **42**, e112165
937 35. Leighton, T. L., Yong, D. H., Howell, P. L., and Burrows, L. L. (2016) Type IV Pilus
938 Alignment Subcomplex Proteins PilN and PilO Form Homo- and Heterodimers *in Vivo*. *J.*
939 *Biol. Chem.* **291**, 19923–19938
940 36. Tammam, S., Sampaleanu, L. M., Koo, J., Sundaram, P., Ayers, M., Chong, P. A., Forman-
941 Kay, J. D., Burrows, L. L., and Howell, P. L. (2011) Characterization of the PilN, PilO and
942 PilP type IVa pilus subcomplex. *Mol. Microbiol.* **82**, 1496–1514
943 37. Geiger, C. J., and O'Toole, G. A. Evidence for the Type IV Pilus Retraction Motor PilT as
944 a Component of the Surface Sensing System in *Pseudomonas aeruginosa*. *J. Bacteriol.* **205**,
945 e00179-23
946 38. Kuchma, S. L., and O'Toole, G. A. (2022) Surface-Induced cAMP Signaling Requires
947 Multiple Features of the *Pseudomonas aeruginosa* Type IV Pili. *J. Bacteriol.* **204**, e00186-
948 22
949 39. Buensuceso, R. N. C., Nguyen, Y., Zhang, K., Daniel-Ivad, M., Sugiman-Marangos, S. N.,
950 Fleetwood, A. D., Zhulin, I. B., Junop, M. S., Howell, P. L., and Burrows, L. L. (2016) The
951 Conserved Tetratricopeptide Repeat-Containing C-Terminal Domain of *Pseudomonas*
952 *aeruginosa* FimV Is Required for Its Cyclic AMP-Dependent and -Independent Functions.
953 *J. Bacteriol.* **198**, 2263–2274
954 40. Buensuceso, R. N. C., Daniel-Ivad, M., Kilmury, S. L. N., Leighton, T. L., Harvey, H.,
955 Howell, P. L., and Burrows, L. L. (2017) Cyclic AMP-Independent Control of Twitching
956 Motility in *Pseudomonas aeruginosa*. *J. Bacteriol.* **199**, e00188-17
957 41. Topal, H., Fulcher, N. B., Bitterman, J., Salazar, E., Buck, J., Levin, L. R., Cann, M. J.,
958 Wolfgang, M. C., and Steegborn, C. (2012) Crystal Structure and Regulation Mechanisms
959 of the CyaB Adenylyl Cyclase from the Human Pathogen *Pseudomonas aeruginosa*. *J.*
960 *Mol. Biol.* **416**, 271–286
961 42. Zhang, Y., Faucher, F., Zhang, W., Wang, S., Neville, N., Poole, K., Zheng, J., and Jia, Z.
962 (2018) Structure-guided disruption of the pseudopilus tip complex inhibits the Type II
963 secretion in *Pseudomonas aeruginosa*. *PLoS Pathog.* **14**, e1007343

964 43. Roberge, N. A., and Burrows, L. L. (2024) Building permits-control of type IV pilus
965 assembly by PilB and its cofactors. *J. Bacteriol.* **206**, e0035924
966 44. Dye, K. J., Vogelaar, N. J., Sobrado, P., and Yang, Z. (2021) High-Throughput Screen for
967 Inhibitors of the Type IV Pilus Assembly ATPase PilB. *mSphere*. **6**, e00129-21
968 45. McDonald-Ramos, J. S., Hicklin, I. K., Yang, Z., and Brown, A. M. (2024) Identification of
969 small molecule inhibitors of the *Chloracidobacterium thermophilum* Type IV Pilus protein
970 PilB by ensemble virtual screening. *Arch. Biochem. Biophys.* 10.1016/j.abb.2024.110127
971 46. Black, W. P., Wang, L., Jing, X., Saldaña, R. C., Li, F., Scharf, B. E., Schubot, F. D., and
972 Yang, Z. (2017) The type IV pilus assembly ATPase PilB functions as a signaling protein
973 to regulate exopolysaccharide production in *Myxococcus xanthus*. *Sci. Rep.* **7**, 7263
974 47. Mancl, J. M., Black, W. P., Robinson, H., Yang, Z., and Schubot, F. D. (2016) Crystal
975 Structure of a Type IV Pilus Assembly ATPase: Insights into the Molecular Mechanism of
976 PilB from *Thermus thermophilus*. *Struct. Lond. Engl. 1993*. **24**, 1886–1897
977 48. Solanki, V., Kapoor, S., and Thakur, K. G. (2018) Structural insights into the mechanism of
978 Type IVa pilus extension and retraction ATPase motors. *FEBS J.* **285**, 3402–3421
979 49. Thongchol, J., Yu, Z., Harb, L., Lin, Y., Koch, M., Theodore, M., Narsaria, U., Shaevitz, J.,
980 Gitai, Z., Wu, Y., Zhang, J., and Zeng, L. (2024) Removal of *Pseudomonas* type IV pili by
981 a small RNA virus. *Science*. **384**, eadl0635
982 50. Qaderi, I., Chan, I., Harvey, H., and Burrows, L. L. (2025) Structural conservation and
983 functional role of TfpY-like proteins in type IV pilus assembly. *J. Bacteriol.* **207**, e00343-
984 24
985 51. Yang, F., Tian, F., Li, X., Fan, S., Chen, H., Wu, M., Yang, C.-H., and He, C. (2014) The
986 degenerate EAL-GGDEF domain protein Filp functions as a cyclic di-GMP receptor and
987 specifically interacts with the PilZ-domain protein PXO_02715 to regulate virulence in
988 *Xanthomonas oryzae* pv. *oryzae*. *Mol. Plant-Microbe Interact. MPMI*. **27**, 578–589
989 52. Chin, K.-H., Kuo, W.-T., Yu, Y.-J., Liao, Y.-T., Yang, M.-T., and Chou, S.-H. (2012)
990 Structural polymorphism of c-di-GMP bound to an EAL domain and in complex with a
991 type II PilZ-domain protein. *Acta Crystallogr. D Biol. Crystallogr.* **68**, 1380–1392
992 53. Qi, Y., Xu, L., Dong, X., Yau, Y. H., Ho, C. L., Koh, S. L., Shochat, S. G., Chou, S.-H.,
993 Tang, K., and Liang, Z.-X. (2012) Functional Divergence of FimX in PilZ Binding and
994 Type IV Pilus Regulation. *J. Bacteriol.* **194**, 5922–5931
995 54. Wang, Y.-C., Chin, K.-H., Tu, Z.-L., He, J., Jones, C. J., Sanchez, D. Z., Yildiz, F. H.,
996 Galperin, M. Y., and Chou, S.-H. (2016) Nucleotide binding by the widespread high-
997 affinity cyclic di-GMP receptor MshEN domain. *Nat. Commun.* **7**, 12481
998 55. Floyd, K. A., Lee, C. K., Xian, W., Nametalla, M., Valentine, A., Crair, B., Zhu, S.,
999 Hughes, H. Q., Chlebek, J. L., Wu, D. C., Hwan Park, J., Farhat, A. M., Lomba, C. J.,
1000 Ellison, C. K., Brun, Y. V., Campos-Gomez, J., Dalia, A. B., Liu, J., Biais, N., Wong, G. C.
1001 L., and Yildiz, F. H. (2020) c-di-GMP modulates type IV MSHA pilus retraction and
1002 surface attachment in *Vibrio cholerae*. *Nat. Commun.* **11**, 1549
1003 56. Aubey, F., Corre, J.-P., Kong, Y., Xu, X., Obino, D., Goussard, S., Lapeyrere, C.,
1004 Souphron, J., Couturier, C., Renard, S., and Duménil, G. (2019) Inhibitors of the *Neisseria*
1005 *meningitidis* PilF ATPase provoke type IV pilus disassembly. *Proc. Natl. Acad. Sci.* **116**,
1006 8481–8486
1007 57. Hughes, H. Q., Christman, N. D., Dalia, T. N., Ellison, C. K., and Dalia, A. B. (2022) The
1008 PilT retraction ATPase promotes both extension and retraction of the MSHA type IVa pilus
1009 in *Vibrio cholerae*. *PLOS Genet.* **18**, e1010561

1010 58. Ellison, C. K., Dalia, T. N., Klancher, C. A., Shaevitz, J. W., Gitai, Z., and Dalia, A. B.
1011 (2021) *Acinetobacter baylyi* regulates type IV pilus synthesis by employing two extension
1012 motors and a motor protein inhibitor. *Nat. Commun.* **12**, 3744
1013 59. Keller, H., Kruse, K., Averhoff, B., Duchardt-Ferner, E., and Wöhnert, J. (2019) NMR
1014 resonance assignments for the GSPII-C domain of the PilF ATPase from *Thermus*
1015 *thermophilus* in complex with c-di-GMP. *Biomol. NMR Assign.* **13**, 361–366
1016 60. Dye, K. J., Salar, S., Allen, U., Smith, W., and Yang, Z. *Myxococcus xanthus* PilB interacts
1017 with c-di-GMP and modulates motility and biofilm formation. *J. Bacteriol.* **205**, e00221-23
1018 61. Dye, K. J., and Yang, Z. (2020) Cyclic-di-GMP and ADP bind to separate domains of PilB
1019 as mutual allosteric effectors. *Biochem. J.* **477**, 213–226
1020 62. Hoang, T. T., Karkhoff-Schweizer, R. R., Kutchma, A. J., and Schweizer, H. P. (1998) A
1021 broad-host-range Flp-*FRT* recombination system for site-specific excision of
1022 chromosomally-located DNA sequences: application for isolation of unmarked
1023 *Pseudomonas aeruginosa* mutants. *Gene*. **212**, 77–86
1024 63. Kilmury, S. L. N., and Burrows, L. L. (2016) Type IV pilins regulate their own expression
1025 via direct intramembrane interactions with the sensor kinase PilS. *Proc. Natl. Acad. Sci.*
1026 **113**, 6017–6022
1027 64. Deatherage, D. E., and Barrick, J. E. (2014) Identification of mutations in laboratory-
1028 evolved microbes from next-generation sequencing data using breseq. *Methods Mol. Biol.*
1029 *Clifton NJ*. **1151**, 165–188
1030 65. Ayers, M., Sampaleanu, L. M., Tammam, S., Koo, J., Harvey, H., Howell, P. L., and
1031 Burrows, L. L. (2009) PilM/N/O/P Proteins Form an Inner Membrane Complex That
1032 Affects the Stability of the *Pseudomonas aeruginosa* Type IV Pilus Secretin. *J. Mol. Biol.*
1033 **394**, 128–142
1034 66. Abramson, J., Adler, J., Dunger, J., Evans, R., Green, T., Pritzel, A., Ronneberger, O.,
1035 Willmore, L., Ballard, A. J., Bambrick, J., Bodenstein, S. W., Evans, D. A., Hung, C.-C.,
1036 O'Neill, M., Reiman, D., Tunyasuvunakool, K., Wu, Z., Žemgulytė, A., Arvaniti, E.,
1037 Beattie, C., Bertolli, O., Bridgland, A., Cherepanov, A., Congreve, M., Cowen-Rivers, A.
1038 I., Cowie, A., Figurnov, M., Fuchs, F. B., Gladman, H., Jain, R., Khan, Y. A., Low, C. M.
1039 R., Perlin, K., Potapenko, A., Savy, P., Singh, S., Stecula, A., Thillaisundaram, A., Tong,
1040 C., Yakneen, S., Zhong, E. D., Zielinski, M., Žídek, A., Bapst, V., Kohli, P., Jaderberg, M.,
1041 Hassabis, D., and Jumper, J. M. (2024) Accurate structure prediction of biomolecular
1042 interactions with AlphaFold 3. *Nature*. **630**, 493–500
1043 67. Meng, E. C., Goddard, T. D., Pettersen, E. F., Couch, G. S., Pearson, Z. J., Morris, J. H.,
1044 and Ferrin, T. E. (2023) UCSF ChimeraX: Tools for structure building and analysis.
1045 *Protein Sci. Publ. Protein Soc.* **32**, e4792
1046 68. Robert, X., and Gouet, P. (2014) Deciphering key features in protein structures with the
1047 new ENDscript server. *Nucleic Acids Res.* **42**, W320-324
1048 69. Ellison, C. K., Kan, J., Dillard, R. S., Kysela, D. T., Ducret, A., Berne, C., Hampton, C. M.,
1049 Ke, Z., Wright, E. R., Biais, N., Dalia, A. B., and Brun, Y. V. (2017) Obstruction of pilus
1050 retraction stimulates bacterial surface sensing. *Science*. **358**, 535–538
1051

1052

1053

1054 **SI Figure Captions**

1055

1056 **Figure S1: Extension regulatory effector mutants produce no detectable surface pili.**
1057 Representative SDS-PAGE of sheared surface proteins. Major pilin subunits (PilA) are indicated.
1058 Sample loading was normalized to flagellin (FliC) levels.

1059

1060 **Figure S2: Mutations which suppress the *fimX* twitching deficit do not confer a growth**
1061 **benefit.** Bacterial growth curves across 18 hours in LB media. Points represent the means of
1062 triplicate samples from three independent experiments ± SD.

1063

1064 **Figure S3: Motility suppressor mutants remain susceptible to pilus-targeting phage PO4.**
1065 Bacterial growth curves across 18 hours in LB media with PO4 phage-challenge. Points
1066 represent the means of triplicate samples from three independent experiments ± SD.

1067

1068 **Figure S4: FimX complementation increases twitching motility in original Δ*fimX***
1069 **suppressor isolates. (A)** Quantification of sub-agar stab twitching motility zones for Δ*fimX*
1070 twitching suppressor mutants complemented with FimX variants. Representative crystal violet-
1071 stained twitching zones are shown to the left. Scale bar = 1 cm. Bars represent the means of
1072 triplicate samples from three independent experiments ± SD. **(B)** Representative colonies
1073 showing pairwise interactions (pink) between FimX and FimX AAA mutant. PilZ was used as a
1074 known non-interacting negative control with FimX (52). Untagged T18/T25 plasmid and PilS-
1075 T18/PilS-T25 homodimers (63) were used as negative and positive controls respectively. **EV**:
1076 empty pHERD30T vector, ***fimX***: *fimX* in pHERD30T vector, **FimX AAA**: FimX AAA in
1077 pHERD30T vector.

1078

1079 **Figure S5: Expression of CyaB *in trans* bypasses the Pil-Chp network to increase twitching**
1080 **motility. (A)** Quantification of sub-agar stab twitching motility zones for a Δ*cyaB* mutant
1081 complemented with CyaB or a catalytically inactive mutant (D234S). Representative CyaB or
1082 CyaB D234S-expressing BTH101 colonies are shown in the inset to the right. Pink colour results
1083 from increased cAMP levels. Representative crystal violet-stained twitching zones are shown to
1084 the left. Bars represent the means of triplicate samples from three independent experiments ± SD.
1085 **(B)** Quantification of sub-agar stab twitching motility zones for a Δ*pilGH* double mutant
1086 complemented with CyaB. Representative twitching zones are shown to the left. Bars represent
1087 the means of triplicate samples from three independent experiments ± SD. All scale bars = 1 cm.
1088 ***: $p \leq 0.001$ (Two-tailed parametric *t*-test). **EV**: empty pHERD30T vector, **His_6-CyaB**
1089 **(D234S)**: N-terminally hexa-histidine tagged CyaB or CyaB D234S in pHERD30T vector.

1090

1091 **Figure S6: Mutants with an mRuby3 cassette insertion upstream of the *pilMNOPQ* operon**
1092 **remain sensitive to pilus-targeting phage PO4.** Bacterial growth curves across 10 hours in LB
1093 media with PO4 phage-challenge. Points represent the means of triplicate samples from two
1094 independent experiments ± SD. **CyaB R456L**: CyaB R456L in pBADGr vector.

1095

1096 **Figure S7: Type II secretion system-dependent clearing on skim milk agar plates for**
1097 **original *fimX* suppressor isolates. (A)** Representative colonies and surrounding zones of
1098 clearance for the Δ*fimX* twitching suppressor mutants. Scale bar = 1 cm. **(B)** Quantification of
1099 the colony area subtracted from the skim milk clearance area. Bars represent the means of
1100 duplicate samples from three independent experiments ± SD. *: $0.05 \geq p \geq 0.01$; ***: $0.001 \geq p$
1101 (Two-tailed parametric *t*-test).

1102

1103 **Figure S8: Alphafold3-predicted models of PilB supressor mutants *pilB* Δ1bp and PilB**
1104 **T430P. (A)** Model of *P. aeruginosa* PilB ($PilB^{Pa}$) monomer. The N1D and linker region (dark
1105 grey), N2D (light blue), and CTD (white) are indicated. The *pilB* Δ1bp C-terminal extension is
1106 shown in dark blue. PilB T430 side chain is shown in stick and in orange. The model PAE plot is
1107 shown to the right. **(B)** *pilB* Δ1bp full length homohexameric Alphafold3 predicted model is
1108 shown below with the extended sequence residues highligted in dark blue. The predicted PilC
1109 interface is shown on the bottom. The N1Ds and linker regions for each monomer are hidden.
1110 The model on the bottom has the two front monomers hidden for clarity. **(C)** X-ray crystal
1111 structure of hexameric PilB from *G. metallireducens* (5TSH) with sequence aligned residues of
1112 interest N429 ($PilB^{Pa}$ T430) and R430 ($PilB^{Pa}$ R431) highlighted in orange and magenta,
1113 respectively. C2-symetric monmers are highlited in the same colours. Dashed lines indicate
1114 approximate protomer interfaces.

1115

1116 **Figure S9: *pilB* Δ1bp constructs complement twitching motility to at least WT levels. (A)**
1117 Quantification of sub-agar stab twitching zone areas of a *pilB*::Tn5 mutant overexpressing *pilB*
1118 Δ1bp 3′ truncations. Representative crystal violet-stained twitching zones are shown to the left.
1119 PilB expression was induced with 0.05% arabinose. Bars represent the means of duplicate
1120 samples from three independent experiments ± SD. **(B)** Quantification of sub-agar stab twitching
1121 zone areas of WT cells overexpressing *pilB* Δ1bp 3′ truncations. Representative twitching zones
1122 are shown to the left. PilB expression was induced with 0.05% arabinose. Bars represent the
1123 means of duplicate samples from three independent experiments ± SD. **EV**: empty pHERD30T
1124 vector, ***pilB* Δ1bp-3 to 21**: *pilB* Δ1bp-3 to 21 in pHERD30T vector. All scale bars = 1 cm. **ns**: p
1125 ≥ 0.05; **: $0.01 \geq p \geq 0.001$ (Two-tailed parametric *t*-test).

1126

1127 **Figure S10: PilB T430X constructs complement twitching motility to at least WT levels. (A)**
1128 Quantification of sub-agar stab twitching zone areas of a *pilB*::Tn5 mutant overexpressing
1129 T430X mutants. Representative crystal violet-stained twitching zones are shown to the left. PilB

expression was induced with 0.05% arabinose. Bars represent the means of duplicate samples from three independent experiments ± SD. **(B)** Quantification of sub-agar stab twitching zone areas of WT cells overexpressing T430X mutants. Representative twitching zones are shown to the left. PilB expression was induced with 0.05% arabinose. Bars represent the means of duplicate samples from three independent experiments ± SD. **PilB T430X**: indicated PilB substitution in pHERD30T vector. All scale bars = 1 cm. **ns**: $p \geq 0.05$; *****: $0.05 \geq p \geq 0.01$ (Two-tailed parametric *t*-test).

Figure S11: PilB T429/431X constructs complement twitching motility. (A) Quantification of sub-agar stab twitching zone areas of a *pilB*::Tn5 mutant overexpressing T429/431X mutants. Representative crystal violet-stained twitching zones are shown to the left. PilB expression was induced with 0.05% arabinose. Bars represent the means of duplicate samples from three independent experiments ± SD. **(B)** Quantification of sub-agar stab twitching zone areas of WT cells overexpressing T429/431X mutants. Representative twitching zones are shown to the left. PilB expression was induced with 0.05% arabinose. Bars represent the means of duplicate samples from three independent experiments ± SD. **PilB T429/431X**: indicated PilB substitution in pHERD30T vector. All scale bars = 1 cm. **ns**: $p \geq 0.05$; *******: $0.001 \geq p$ (Two-tailed parametric *t*-test).

Figure S12: Purified ΔN1D-His$_6$-PilB and FimX protein samples. SDS-PAGE of representative protein samples used in the study. Samples are diluted to the same concentrations added to the reaction mixture preparation.

Figure S13: PilA A86C mutants retain twitching motility. Quantification of sub-agar stab twitching zone areas of PilA A86C mutants. Representative crystal violet stained twitching zones are shown to the left. Bars represent the means of triplicate samples from three independent experiments ± SD. Scale bar = 1 cm.

Figure S14: Vector control assays for FimX localization studies. (A) Quantification of sub-agar stab twitching zone areas of Δ*fimX* mutants complemented with N-terminal fusion of mNeonGreen (mNGr) to FimX. Representative crystal violet stained twitching zones are shown to the left. Expression was not induced with arabinose. Bars represent the means of triplicate samples from three independent experiments ± SD. Scale bar = 1 cm. **EV**: empty pHERD30T, **mNGr-FimX (AAA)**: N-terminal fusion of mNeonGreen to FimX or FimX AAA in pHERD30T vector. **(B)** Representative images of Δ*fimX* mutant cells carrying empty pHERD30T with background fluorescence subtracted. Scale bar = 2 μm. *******: $0.001 \geq p$ (Two-tailed parametric *t*-test).

1168 **Figure S15: PilB mutations contributing to enhanced twitching motility in Δ*fimX* are rare.**
1169 **(A)** Total protein sequence length of PilB orthologues in *P. aeruginosa* from the
1170 *Pseudomonas*.com database. Sequences which are the same length as PAO1 PilB (566 residues)
1171 are indicated in blue. **(B)** Percentage of sequences with an identifiable α-helix-disrupting residue
1172 ± three amino acids from the position which aligns with PAO1 PilB T430.

1173

1174

1175

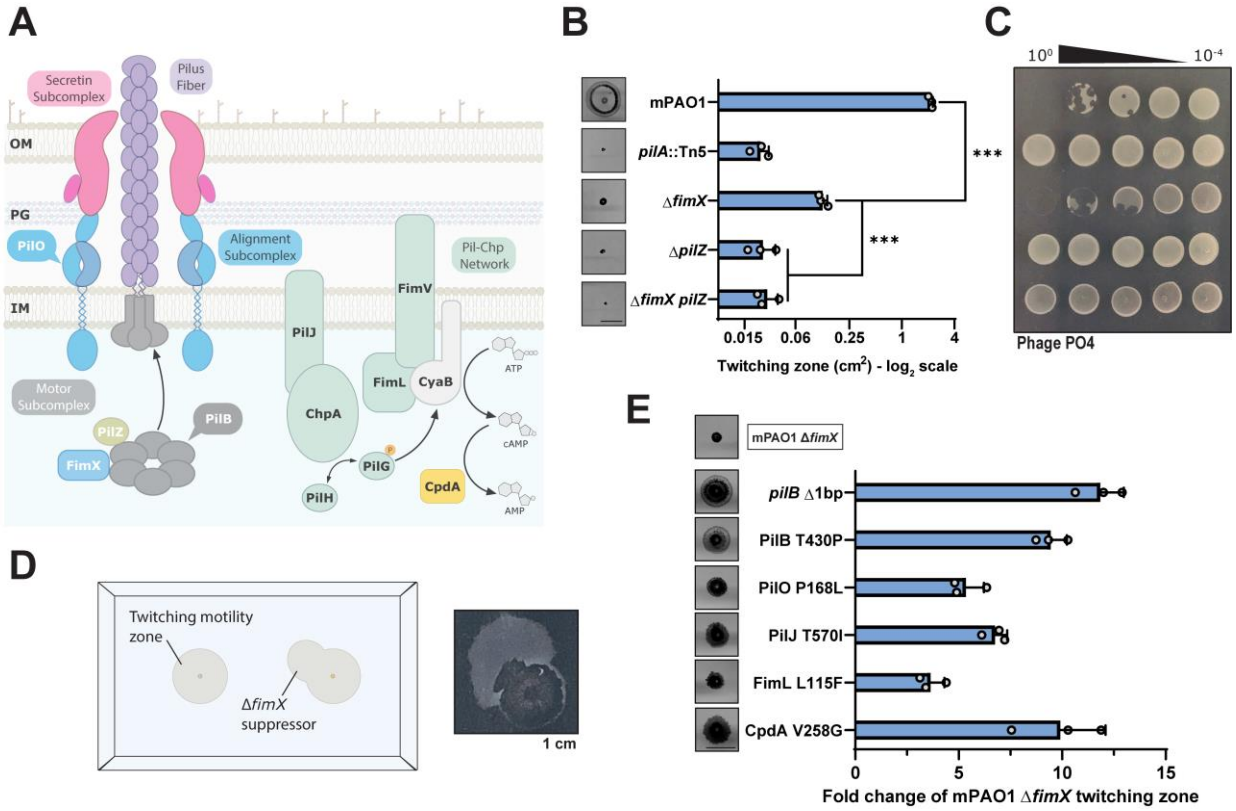
A
Secretin Subcomplex
Pilus Fiber
OM
PG
PilO
Alignment Subcomplex
Pil-Chp Network
IM
FimV
PilJ
FimL
CyaB
ATP
Motor Subcomplex
PilZ
PilB
ChpA
cAMP
FimX
PilG
CpdA
PilH
AMP
B
mPAO1
pilA::Tn5
ΔfimX
ΔpilZ
ΔfimX pilZ
***
***
0.015
0.06
0.25
1
4
Twitching zone (cm2) - log2 scale
C
10⁰
10⁻⁴
Phage PO4
D
Twitching motility zone
ΔfimX suppressor
1 cm
E
mPAO1 ΔfimX
pilB Δ1bp
PilB T430P
PilO P168L
PilJ T570I
FimL L115F
CpdA V258G
0
5
10
15
Fold change of mPAO1 ΔfimX twitching zone

Fig 1

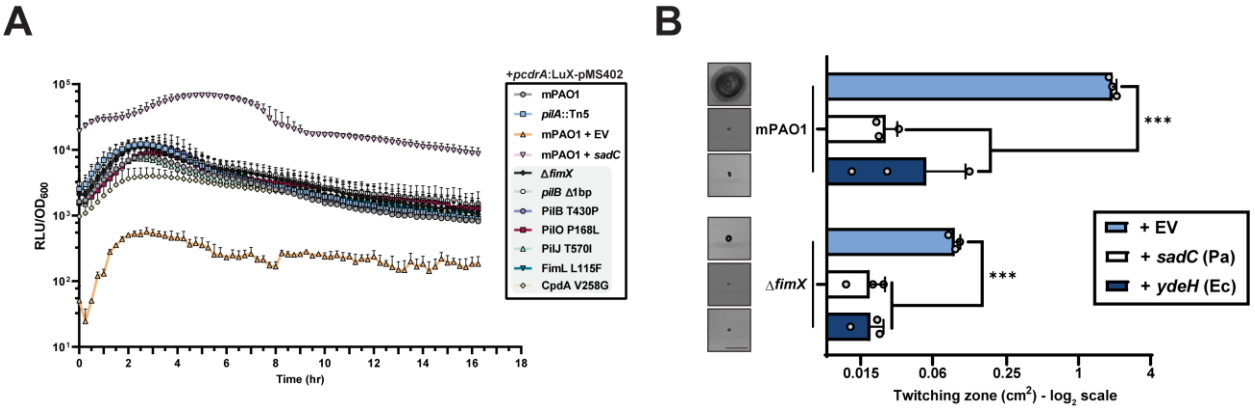
A
+pcdrA:LuX-pMS402
mPAO1
pilA::Tn5
mPAO1 + EV
mPAO1 + sadC
ΔfimX
pilB Δ1bp
PilB T430P
PilO P168L
PilJ T570I
FimL L115F
CpdA V258G
RLU/OD600
Time (hr)
B
mPAO1
ΔfimX
***
***
+ EV
+ sadC (Pa)
+ ydeH (Ec)
0.015
0.06
0.25
1
4
Twitching zone (cm2) - log2 scale

Fig 2

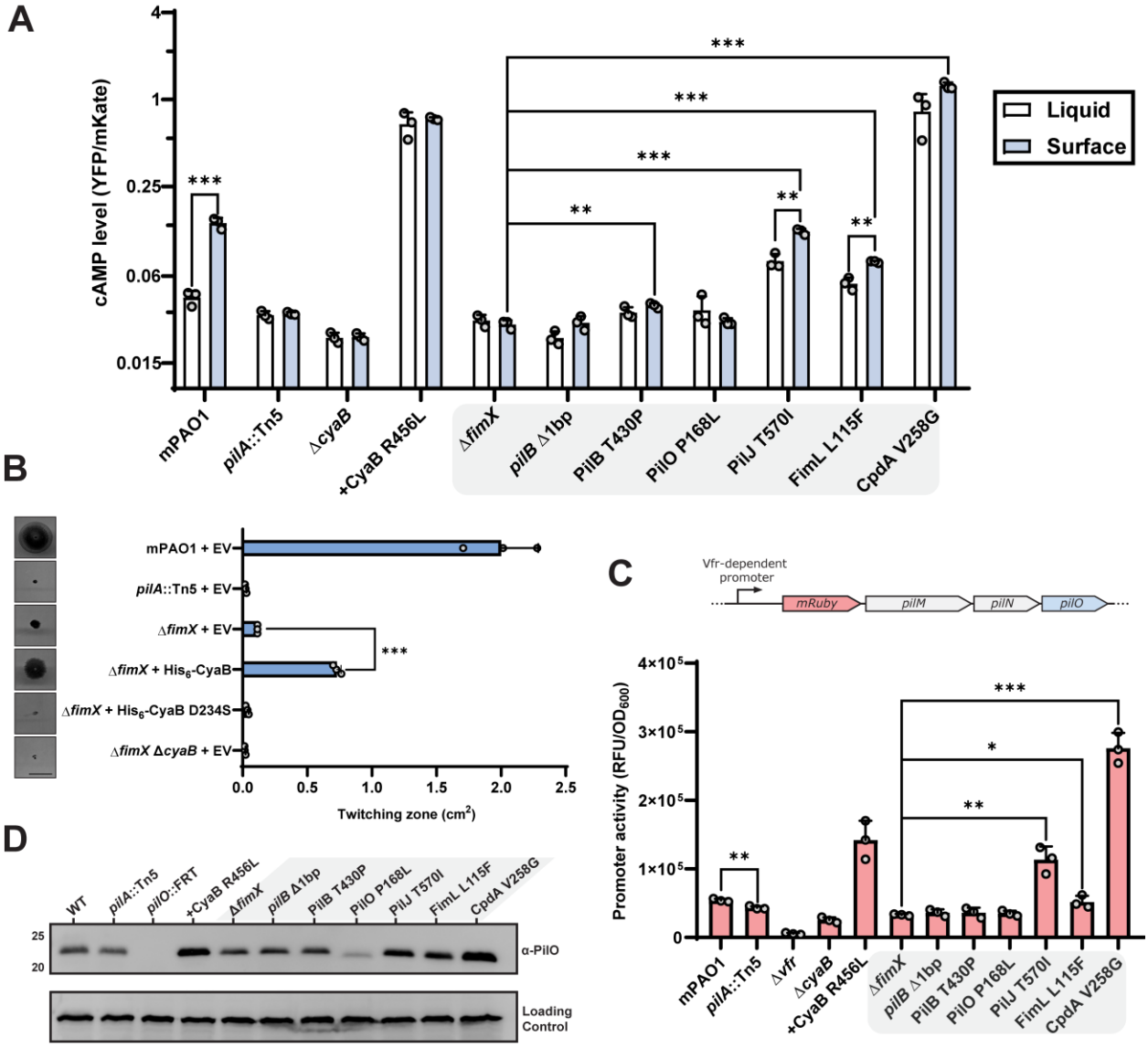
A
cAMP level (YFP/mKate)
4
1
0.25
0.06
0.015
Liquid
Surface
mPAO1
pilA::Tn5
ΔcyaB
+CyaB R456L
ΔfimX
pilB Δ1bp
PilB T430P
PilO P168L
PilJ T570I
FimL L115F
CpdA V258G
B
mPAO1 + EV
pilA::Tn5 + EV
ΔfimX + EV
ΔfimX + His6-CyaB
ΔfimX + His6-CyaB D234S
ΔfimX ΔcyaB + EV
Twitching zone (cm2)
C
Vfr-dependent promoter
mRuby
pilM
pilN
pilO
Promoter activity (RFU/OD600)
4×10^5
3×10^5
2×10^5
1×10^5
0
mPAO1
pilA::Tn5
Δvfr
ΔcyaB
+CyaB R456L
ΔfimX
pilB Δ1bp
PilB T430P
PilO P168L
PilJ T570I
FimL L115F
CpdA V258G
D
WT
pilA::Tn5
pilO::FRT
+CyaB R456L
ΔfimX
pilB Δ1bp
PilB T430P
PilO P168L
PilJ T570I
FimL L115F
CpdA V258G
25
20
α-PilO
Loading Control

Fig 3

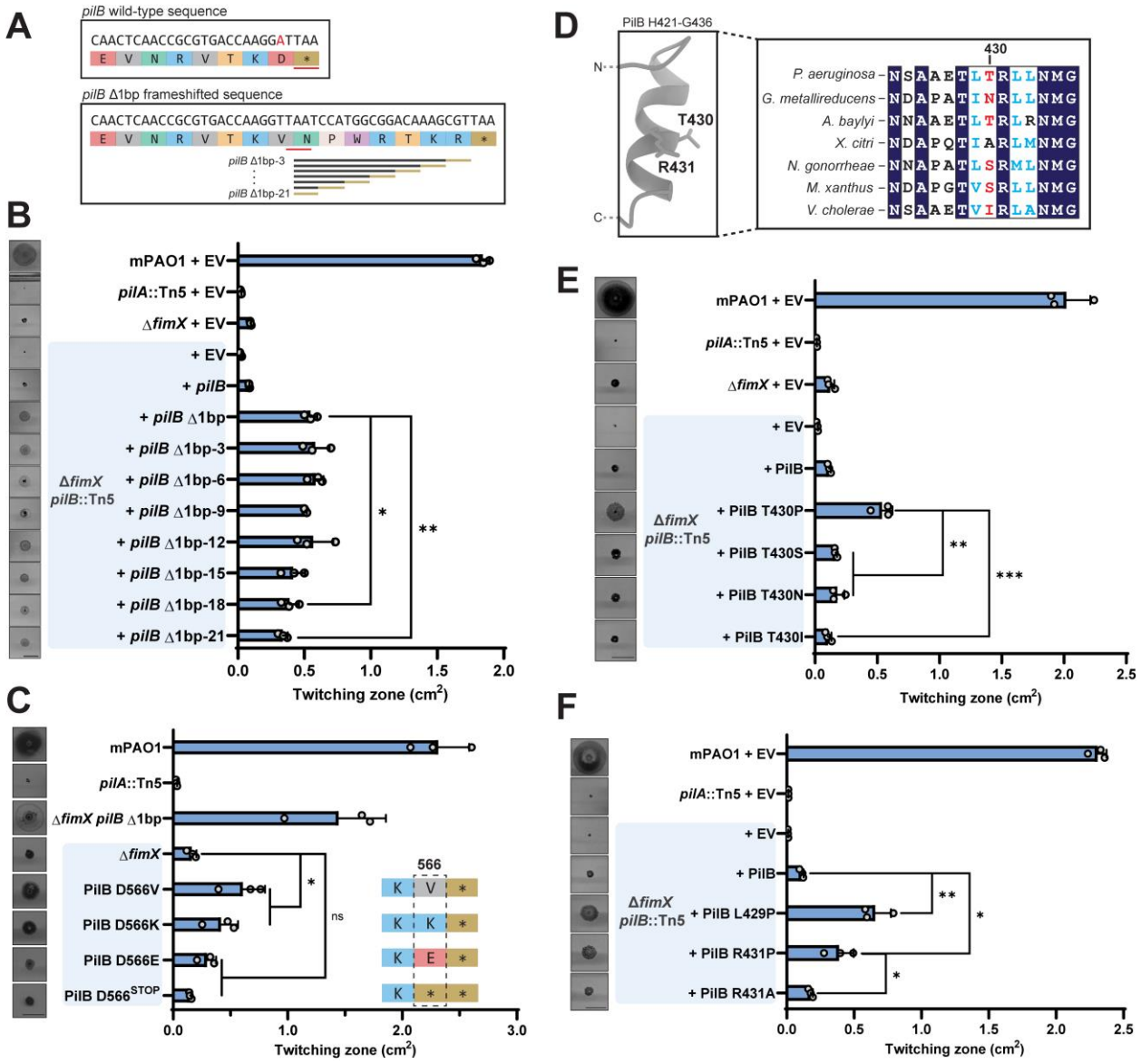
A
pilB wild-type sequence
CAACTCAACCGCGTGACCAAGGATTAA
E V N R V T K D *
pilB Δ1bp frameshifted sequence
CAACTCAACCGCGTGACCAAGGTTAATCCATGGCGGACAAAGCGTTAA
E V N R V T K V N P W R T K R *
pilB Δ1bp-3
pilB Δ1bp-21
B
mPAO1 + EV
pilA::Tn5 + EV
ΔfimX + EV
+ EV
+ pilB
+ pilB Δ1bp
+ pilB Δ1bp-3
+ pilB Δ1bp-6
+ pilB Δ1bp-9
+ pilB Δ1bp-12
+ pilB Δ1bp-15
+ pilB Δ1bp-18
+ pilB Δ1bp-21
ΔfimX pilB::Tn5
Twitching zone (cm2)
C
mPAO1
pilA::Tn5
ΔfimX pilB Δ1bp
ΔfimX
PilB D566V
PilB D566K
PilB D566E
PilB D566STOP
566
K V *
K K *
K E *
K * *
ns
Twitching zone (cm2)
D
PilB H421-G436
N
C
T430
R431
430
P. aeruginosa – NSAAETLTRLLNMG
G. metallireducens – NDAPATINRLLNMG
A. baylyi – NNAAETLTRLRNMG
X. citri – NDAPQTIARLMNMG
N. gonorrheae – NNAPATLSRMLNMG
M. xanthus – NDAPGTVSRLLNMG
V. cholerae – NSAAETVIRLANMG
E
mPAO1 + EV
pilA::Tn5 + EV
ΔfimX + EV
+ EV
+ PilB
+ PilB T430P
+ PilB T430S
+ PilB T430N
+ PilB T430I
ΔfimX pilB::Tn5
Twitching zone (cm2)
F
mPAO1 + EV
pilA::Tn5 + EV
+ EV
+ PilB
+ PilB L429P
+ PilB R431P
+ PilB R431A
ΔfimX pilB::Tn5
Twitching zone (cm2)

Fig 4

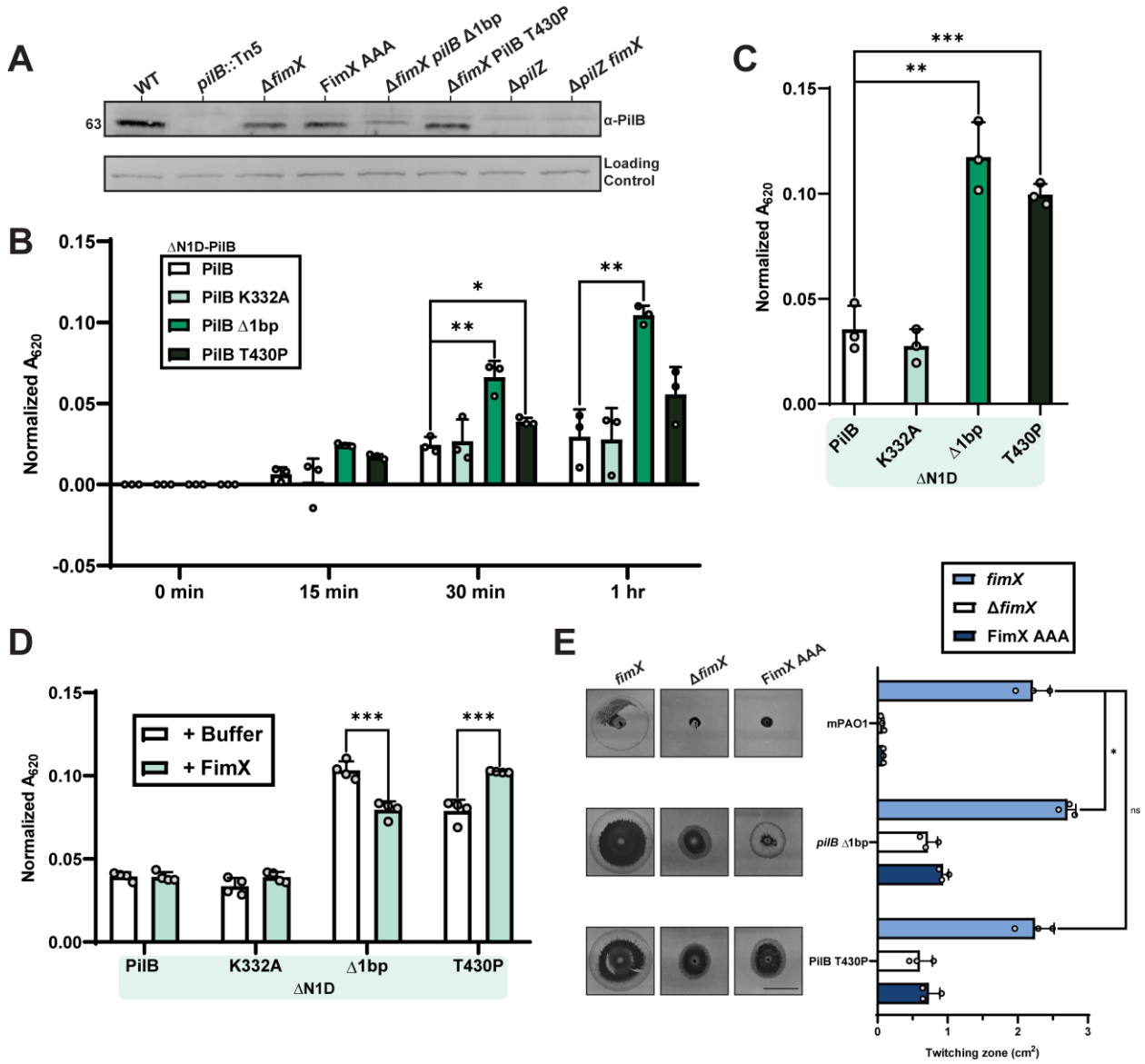
A
WT
pilB::Tn5
ΔfimX
FimX AAA
ΔfimX pilB Δ1bp
ΔfimX PilB T430P
ΔpilZ
ΔpilZ fimX
63
α-PilB
Loading Control
B
ΔN1D-PilB
PilB
PilB K332A
PilB Δ1bp
PilB T430P
Normalized A620
0 min
15 min
30 min
1 hr
C
Normalized A620
PilB
K332A
Δ1bp
T430P
ΔN1D
D
+ Buffer
+ FimX
Normalized A620
PilB
K332A
Δ1bp
T430P
ΔN1D
E
fimX
ΔfimX
FimX AAA
mPAO1
pilB Δ1bp
PilB T430P
Twitching zone (cm2)
ns

Fig 5

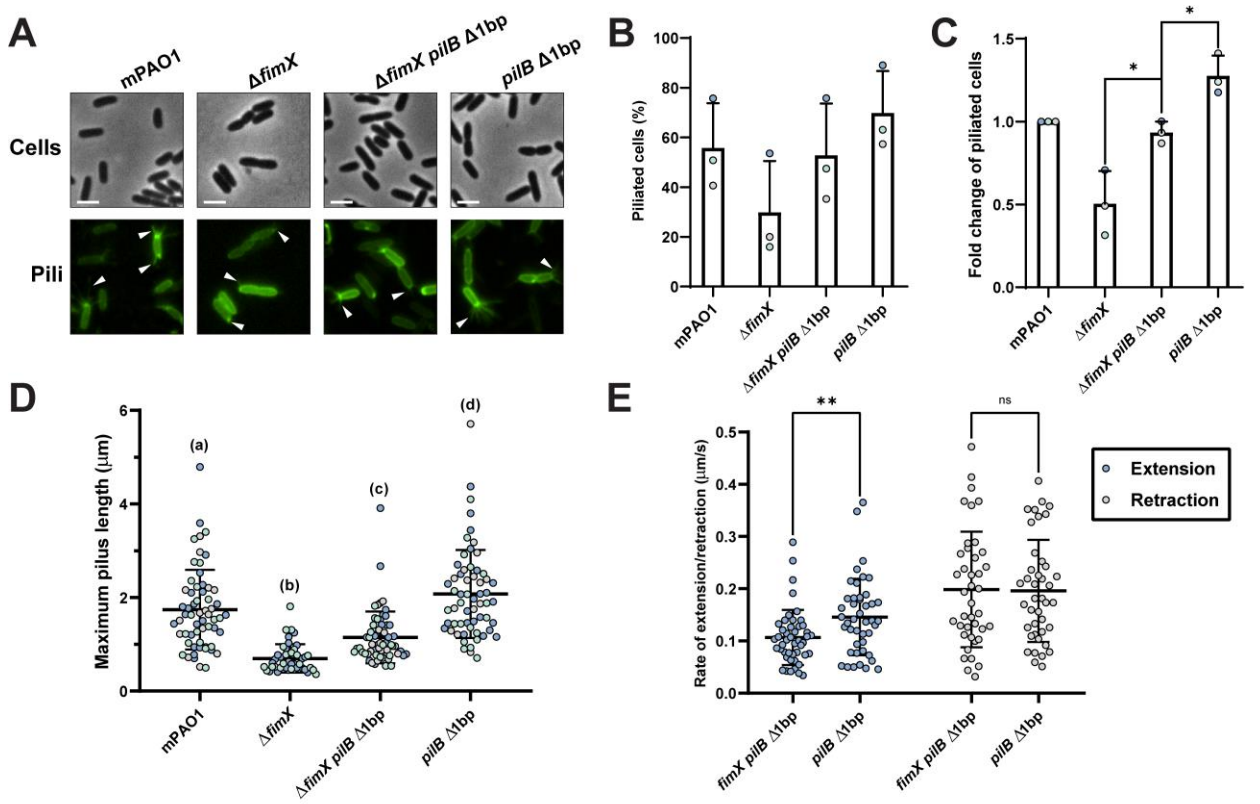
A
mPAO1
ΔfimX
ΔfimX pilB Δ1bp
pilB Δ1bp
Cells
Pili
B
Piliated cells (%)
mPAO1
ΔfimX
ΔfimX pilB Δ1bp
pilB Δ1bp
C
Fold change of piliated cells
D
Maximum pilus length (μm)
(a)
(b)
(c)
(d)
E
Rate of extension/retraction (μm/s)
**
ns
Extension
Retraction
fimX pilB Δ1bp
pilB Δ1bp

Fig 6

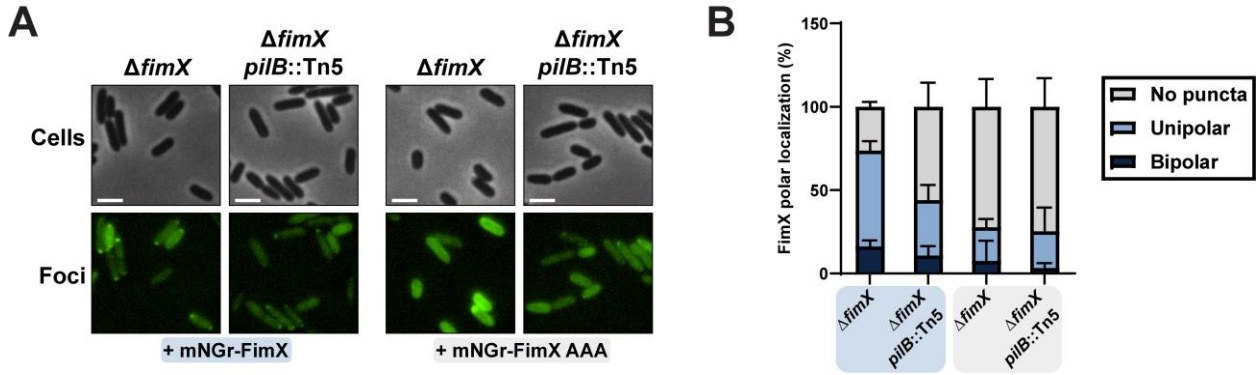
A
ΔfimX
ΔfimX pilB::Tn5
ΔfimX
ΔfimX pilB::Tn5
Cells
Foci
+ mNGr-FimX
+ mNGr-FimX AAA
B
FimX polar localization (%)
No puncta
Unipolar
Bipolar
ΔfimX
ΔfimX pilB::Tn5
ΔfimX
ΔfimX pilB::Tn5

Fig 7

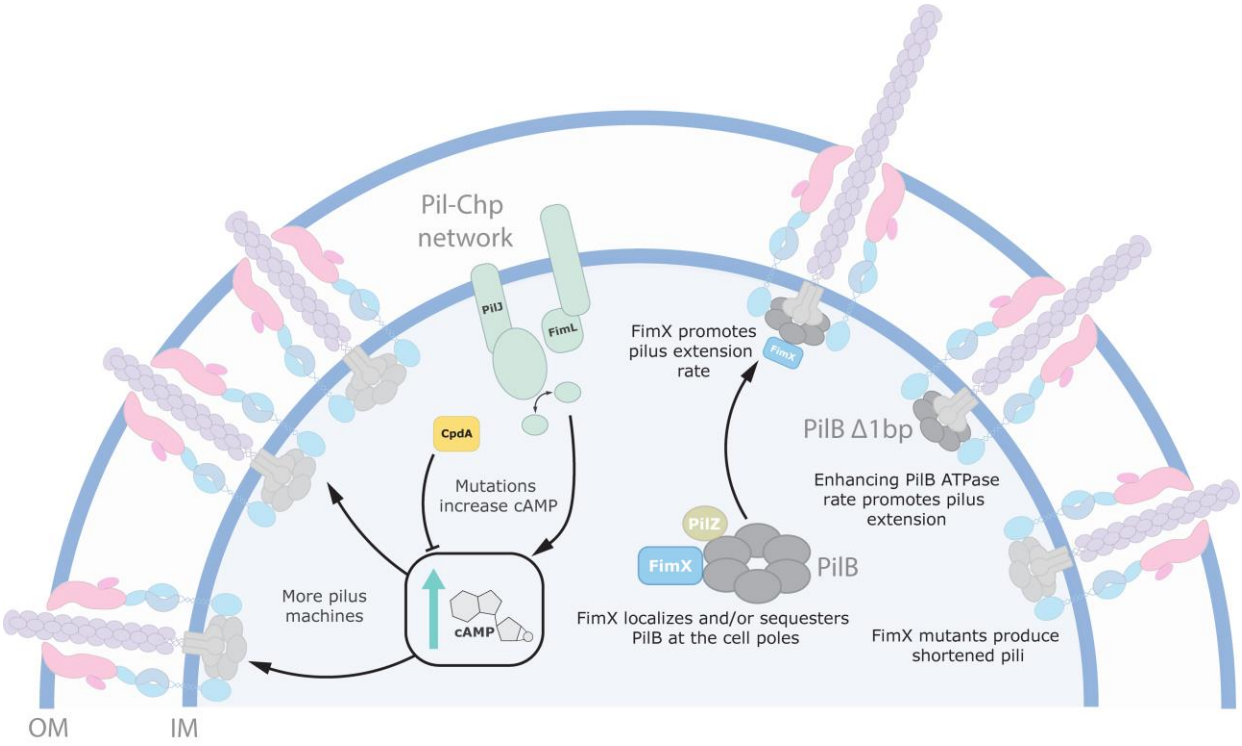
Pil-Chp
network
PilJ
FimL
CpdA
Mutations
increase cAMP
More pilus
machines
cAMP
FimX promotes
pilus extension
rate
FimX
PilB Δ1bp
Enhancing PilB ATPase
rate promotes pilus
extension
PilZ
FimX
PilB
FimX localizes and/or sequesters
PilB at the cell poles
FimX mutants produce
shortened pili
OM
IM

Fig 8